

4-22-2021 4:00 PM

Biomechanical strategies to reduce subsidence in Posterior Lumbar Interbody Fusion procedures

Renan Jose Rodrigues Fernandes, *The University of Western Ontario*

Supervisor: Bailey, Christopher S, *The University of Western Ontario*

Co-Supervisor: Zdero, Radovan, *The University of Western Ontario*

Co-Supervisor: Rasoulinejad, Parham, *The University of Western Ontario*

A thesis submitted in partial fulfillment of the requirements for the Master of Science degree in Surgery

© Renan Jose Rodrigues Fernandes 2021

Follow this and additional works at: <https://ir.lib.uwo.ca/etd>



Part of the [Orthopedics Commons](#)

Recommended Citation

Rodrigues Fernandes, Renan Jose, "Biomechanical strategies to reduce subsidence in Posterior Lumbar Interbody Fusion procedures" (2021). *Electronic Thesis and Dissertation Repository*. 7760.
<https://ir.lib.uwo.ca/etd/7760>

This Dissertation/Thesis is brought to you for free and open access by Scholarship@Western. It has been accepted for inclusion in Electronic Thesis and Dissertation Repository by an authorized administrator of Scholarship@Western. For more information, please contact wlsadmin@uwo.ca.

Biomechanical strategies to reduce subsidence in PLIF procedures

Renan Jose Rodrigues Fernandes

Abstract

Posterior approaches remain among the most used to perform lumbar interbody fusion (LIF) surgery. It happens because of the advantage of providing direct access to the neural elements in the lumbar spine and the surgeons' preference for the approach. But the interbody fusion devices (IFD) inserted using posterior approaches are of limited size, and implant subsidence remains the most common complication after LIF surgery. It can be catastrophic for the patient resulting in worse outcomes or even requiring revision surgery. Since increasing the cage's size is not possible in PLIF surgeries, this thesis will explore biomechanical strategies to increase the load distribution across the IFD and reduce the risk of subsidence. It will be done using patient-specific devices, matching the bony endplate anatomy, manufactured through rapid prototyping and exploring the role of the bone graft housed inside the cage to increase load sharing.

Keywords

Subsidence, Biomechanics, Lumbar Interbody Fusion, Interbody fusion device, Cage, Spine surgery, Patient-specific, Lumbar spine, Rapid prototyping, Bone graft

Summary for lay audience

Different techniques promote bone fusion between the vertebrae on the spine in posterior lumbar spine surgery. One of the most used methods is called interbody fusion, which involves removing the intervertebral body disc, meaning the soft material located between the bones of the spine. After this soft material is removed, a device containing a bone graft is usually inserted inside the disc space to promote bone fusion between the superior and the inferior vertebra of the spine. This device is referred to as "cage" and has different purposes, like increasing the space for the spine's neural elements (i.e. nerves) and promoting a better alignment for the lumbar spine. But one of the biggest problems after inserting those devices into the disc space is that they can sink into the vertebral body over time. This is called subsidence. When it occurs, it can trigger the new onset of leg pain and back pain for the patients, resulting in worse outcomes.

Usually, the cages are produced having a similar size and shape for all the patients. The present study proposes investigating if the development of a device that matches the bone geometry of the patient's own vertebra is better than using a "one size fits all" device that suits everyone and can reduce the risk for device subsidence. The purpose of the testing is to figure out which kind of device will subside more easily into the bone under compressive load. This biomechanical study involved using a mechanical loading frame to test the implants created to compare to commercial implants. Another goal for the study was to investigate if the bone graft inserted inside these devices can help prevent subsidence. We will use spine vertebrae from people that have donated their bodies for research. This research will be informative to spine surgeons with the first biomechanical evidence to date regarding this subject. The results of this study will draw the attention of the scientific

community to an important topic regarding surgical complications that occurs in approximately 15% of surgeries and will present a possible solution to the problem.

Acknowledgments

I could not fail to acknowledge and thank the contribution of many people to this project.

To my supervisors, Dr. Chris Bailey, Dr. Radovan Zdero and Dr. Parham Rasoulinejad, for their expert opinions and inputs in every step and for providing the resources for completing this project.

I want to thank Dr. Andrew Kanawati for the friendship, patience and assistance in teaching me how to use 3D slicer software and the help during the 3D printing process and bone cleaning.

To Aaron Gee, for the friendship, patience and assistance in teaching me how to use SolidWorks and ImageJ software and the help during the 3D printing process and biomechanical testing.

To the CT-technicians at University Hospital, that made possible the cadavers' scanning process after business hours.

To the families that anonymously donate their beloveds one's bodies for research.

Declaration of conflict of interests

The author has no potential conflicts of interest concerning the research presented in this thesis.

Funding

This research received funding through Lawson's Internal Research Fund (IRF 19-19).

Contributions

Renan Fernandes – Primary author, responsible for conceiving ideas, methodology design, conducting experiments, data collection, statistical analysis, and drafting the manuscript.

Chris Bailey - Supervisor, provided access to research components, expert opinion about spine surgery and biomechanics, and provided revisions to the manuscript's scientific content.

Radovan Zdero - Supervisor, provided access to research components, expert opinion about biomechanics, and provided revisions to the manuscript's scientific content.

Parham Rasoulinejad - Supervisor, provided access to research components and helped in the methodology design.

Aaron Gee - Experimental design, performed experiments, data collection, provided revisions to the manuscript's scientific content.

Andrew Kanawati – Experimental design and provided revisions to the manuscript's scientific content.

Table of Contents

Abstract.....	ii
Keywords.....	ii
Summary for lay audience	iii
Acknowledgments.....	v
Declaration of conflict of interests	vi
Funding	vi
Contributions	vi
Chapter 1 – Introduction.....	1
Historical overview in spinal surgery	1
Lumbar interbody fusion (LIF).....	2
LIF Approaches	2
<i>Figure 1.</i>	3
Complications related to LIF.	4
Human lumbar vertebrae	5
<i>Figure 2</i>	6
Interbody fusion devices.....	7
<i>Figure 3.</i>	8
Rapid prototyping	9
<i>Figure 4.</i>	10
Research goals	11
References	13
Chapter 2 - Biomechanical evaluation of morselized bone graft for preventing interbody fusion device subsidence.	15
Introduction/Background	15
Methodology.....	16
<i>Figure 1.</i>	18
Results.....	20
<i>Table 1.</i>	21
<i>Figure 2.</i>	22
<i>Figure 3</i>	22
Discussion.....	23

Conclusion.....	25
References	26
Chapter 3 – Biomechanical evaluation of the amount of congruent bone endplate and 3d printed patient-specific PLIF cage vs commercial cage.....	28
Introduction	28
Methodology.....	29
<i>Figure 5</i>	31
<i>Figure 6</i>	33
<i>Figure 7</i>	34
<i>Figure 8</i>	35
<i>Figure 9</i>	36
<i>Figure 10</i>	37
<i>Table 2</i>	38
<i>Figure 11</i>	40
Results.....	41
<i>Table 3</i>	42
<i>Table 4</i>	43
<i>Figure 12</i>	43
Discussion.....	44
Conclusion.....	46
References	47
Chapter 4 – Biomechanical comparison of subsidence between patient-specific and non-patient-specific PLIF cages.....	49
Introduction	49
Methodology.....	50
<i>Figure 13</i>	52
<i>Figure 14</i>	54
<i>Figure 15</i>	55
<i>Figure 16</i>	56
<i>Figure 17</i>	57
<i>Figure 18</i>	58
<i>Figure 19</i>	60
Results.....	60
<i>Table 5</i>	62

<i>Table 6</i>	62
<i>Figure 20</i>	63
<i>Figure 21</i>	64
Discussion.....	65
Conclusion.....	68
References	69
Chapter 5 – Conclusion and future directions	71
Appendix A.....	73
Pressure-sensitive film calibration.....	73
Curriculum Vitae	74

Chapter 1 – Introduction

Historical overview in spinal surgery

As the population ages, degenerative spine diseases are increasing, and so is the number of spine surgeries performed(1).

Spine surgery started to be described in the late 19th century. Initially, the spine fixation methods were rudimentary and were performed through the usage of steel rods and wiring techniques, but due to such constructs' weaknesses, frequently, the patients were kept immobilized using plaster or an external orthosis(2).

In the early 20th century, fusion procedures to treat several spinal pathologies were reported and involved the use of autografts and a combination of osteotomies to promote bone healing and fusion. Due to the lack of efficient fixation techniques, pseudoarthrosis remained the main factor of adverse surgical outcomes; furthermore, the material used also frequently resulted in hardware failure secondary to corrosion(2).

It was not until the mid-20th century that spinal fusion techniques became disseminated, and they were boosted by the publication of the first proposed treatment for herniated discs. Later, two interbody fusion procedures were described to improve spinal fusion by bone graft placement inside the disc space. Concurrently, titanium emerged around the same age as a material of choice for orthopedic spinal implants(2).

During this time that spine fixation techniques were evolving with the introduction of titanium and the introduction of pedicle screws, the use of interbody fusion device was only experimentally described in animals. In 1989, the first procedure using a titanium interbody cage in humans was described(2).

Lumbar interbody fusion (LIF)

Since its initial introduction, LIF has become widely used to treat different pathologies in the lumbar spine, including degenerative scoliosis, spinal stenosis, spondylolisthesis, and degenerative disc disease.

The procedure involves the placement of a spinal disc spacer, usually an interbody cage housing bone graft, to facilitate fusion between two vertebral bodies. It is done after removing the disc's nucleus pulposus and the endplate's cartilaginous portion (3, 4).

The added advantage of LIF surgery is that it also restores the disc space height, thus directly and indirectly decompressing neural elements(5). This has improved fusion rates, helped correct deformities, improved coronal and sagittal balance, and established mechanical stability(4, 6).

Several techniques are available to approach the interbody space, and a variety of factors influence which approach will be chosen, including patient, procedural and surgeon. Perhaps, the primary factor considered is the surgeon's familiarity with the approach. Not all surgeons are familiar with all techniques, and for surgeons, certain techniques may require an access surgeon's aid, with potentially limited availability. Other factors to be considered are the lumbar spine level, the number of levels requiring treatment, disease etiology (e.g., the necessity of decompression of anterior or posterior elements of the spine), bone quality, and patient's associated diseases(3, 5).

LIF Approaches

Currently, five main approaches are being used for lumbar interbody fusion (Figure 1): anterior lumbar interbody fusion (ALIF), oblique lumbar interbody fusion (OLIF), lateral interbody fusion (LLIF), transforaminal lumbar interbody fusion (TLIF), and posterior lumbar interbody fusion (PLIF) (3).

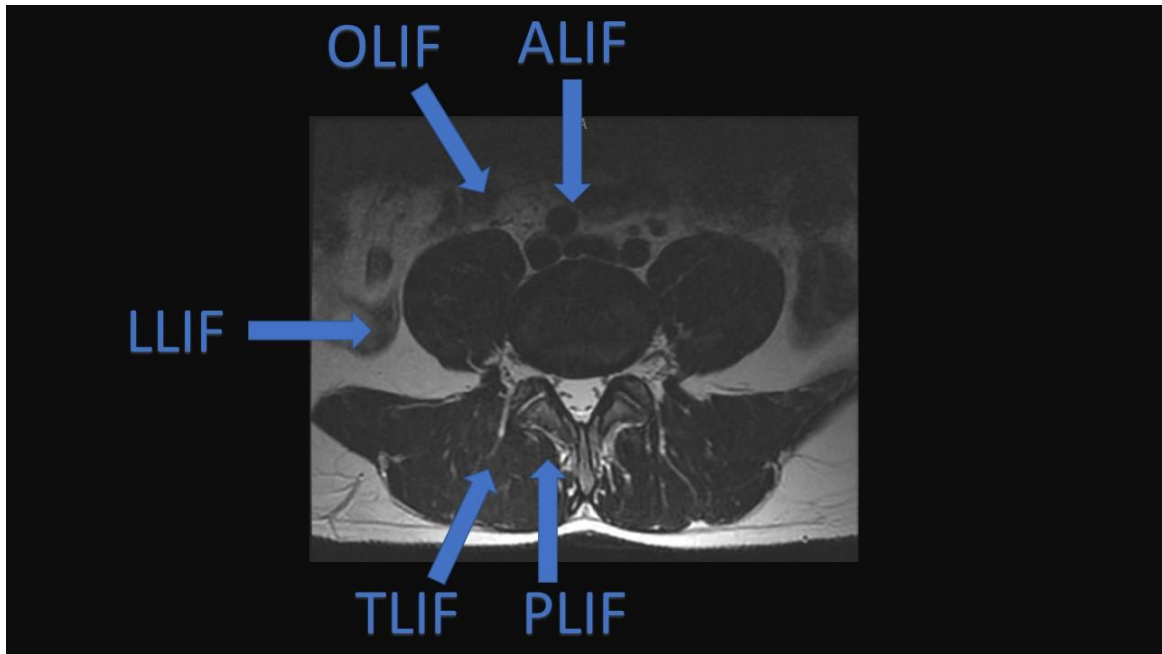


Figure 1. Surgical approaches for lumbar interbody fusion (LIF) techniques: Anterior (ALIF), Oblique (OLIF), Lateral (LLIF), Transforaminal (TLIF) and Posterior (PLIF).

Although related to the direction of approach, the existing methods can be categorized in anterior options (ALIF/OLIF/LLIF), when located anterior to the transverse process, and posterior options (PLIF/TLIF), when located posterior to the transverse process(3).

From a surgical perspective, each technique has its advantages and disadvantages. Anterior approaches have the benefit of providing a direct view of the disc space, and they have a more prominent dissection corridor, allowing placement of bigger cages. However, anterior approaches don't provide direct access to the posterior elements or neural

structures, relying on indirect decompression in many cases(5). On the other hand, posterior approaches are more suitable for the visualization of neural structures and direct spinal canal decompression. However, the disc space access is more limited by the dural tube, and consequently, the cage placed in the interbody space is of smaller size(5).

OLIF, TLIF, and PLIF can be used satisfactorily in every lumbar spine segment. However, LLIF is inappropriate for the L5/S1 level, and ALIF is usually not an option above L3 due to vascular anatomy restrictions (3).

PLIF or TLIF approaches accounted for between 79 to 86% of all LIFs performed in the United States between 2001 and 2010(7). Among the reasons to explain their common uses are surgeon familiarity, lower complication rates and mortality, lower cost, and shorter hospitalization length compared to anterior options(7).

Complications related to LIF.

The most common complications related to LIF that require revision surgery are postoperative infections, non-fusion (commonly called pseudoarthrosis), and subsidence.

Deep wound infections after LIF are reported to be around 2-18% and are usually treated with antibiotics, debridement, and implant removal when needed. Regardless of the approach used, no difference in infection rates was shown among techniques(3, 8, 9).

Pseudoarthrosis or non-fusion is a concern and sometimes requires revision surgery. Fusion rates have increased over time due to cages improvements in materials and design and range from 89%(LLIF) to 95%(ALIF) after LIF procedures(6).

However, the complication of implant subsidence remains the most common challenge to be overcome after LIF. Subsidence occurs when the cage penetrates one or

both adjacent vertebral bodies' endplates. Subsidence rates range from 7% to 38%(10) and are dependent on implant size, the approach used, bone mineral density (BMD), and endplate morphology(11-14). PLIF cages have been shown to have lower subsidence rates when compared to other techniques, attributed to the fact that two cages inserted on the endplate can promote better load sharing(10). After subsidence, the clinical outcomes can worsen, resulting in increased pain and loss of the desired effect of indirect decompression of the neural elements and sagittal balance(12). A comparative study examining different cages types showed that after subsidence occurred, it was more likely to continue evolving, leading to delayed bone fusion or even pseudarthrosis with pedicle screw loosening(10).

Although subsidence mechanisms are not fully understood, to avoid implant subsidence, the mismatch between the endplate properties and cage properties must be reduced to improve the strength between the vertebra-device interface(15). Vertebral body characteristics seem to be an essential factor in preventing subsidence.

Human lumbar vertebrae

The human lumbar vertebra can be divided into two regions, which comprise the vertebral body and the posterior elements. The vertebral body is a cylindrical shaped structure framed by an external cortical bone shell and internal cancellous bone. The posterior elements comprise the pars interarticularis, facet joints, and transverse and spinous processes.

The vertebral endplates are located at the superior and inferior aspects of the vertebral body. They consist of a central portion of thin and porous cortical bone, over top of which is located cartilaginous component. On the outer periphery of the endplate is located the

epiphyseal rim, framed by a more robust bone. The intervertebral disc's annulus fibrosus attaches to this peripheral epiphyseal rim, while the nucleus pulposus is restrained centrally, between two adjacent cartilaginous endplates (Figure 2).

Several studies have improved the understanding of the endplate morphology. Endplate morphology can be classified into three different types: concave, flat, or irregular, and is based on radiologic images obtained from X-ray, CT-scans, or MRI. The superior and inferior endplates are not symmetric, with variation in size and depth among patients, and variable thickness of the epiphyseal rim is different depending on vertebral level(16, 17).

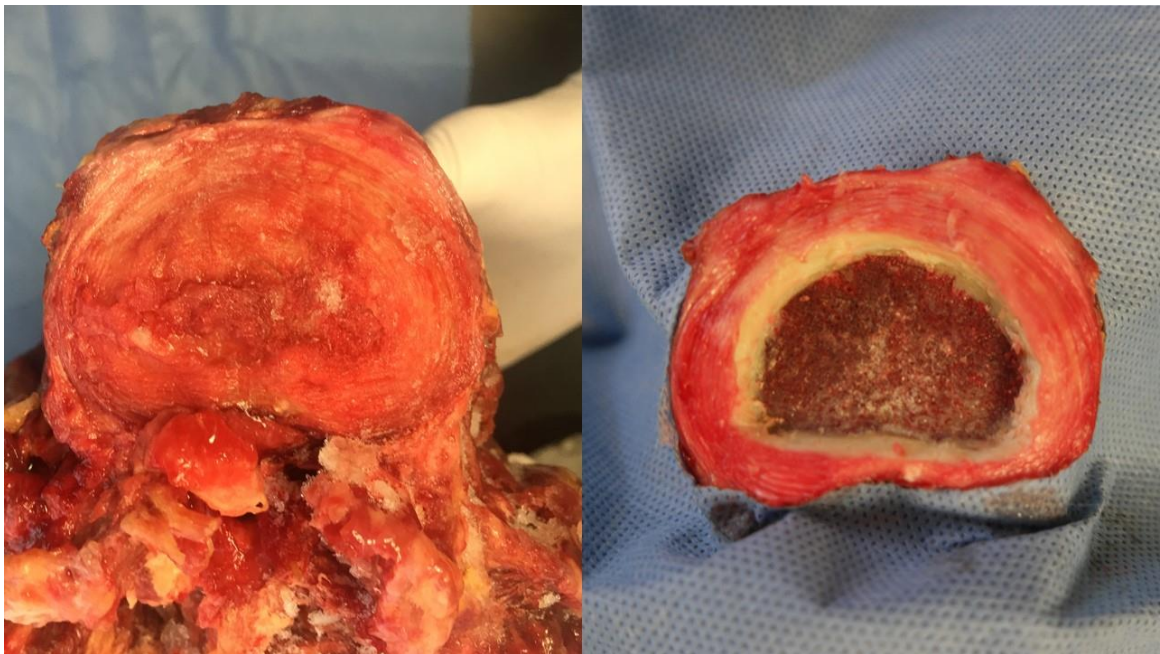


Figure 2. Pictures showing the morphology of the intervertebral disc. The left side picture shows the peripheral annulus fibrosus and the central nucleus pulposus; on the right side, the nucleus pulposus was removed.

The endplate thickness increases toward the periphery, with several studies demonstrating that the stiffness and strength are weaker in the central portion of the

endplate compared to the posterolateral portion of the endplates. Moreover, low BMD and disc degeneration can affect the endplates' strength over time compared to healthy endplates(18, 19). Thus, spinal implants that load the periphery of the endplates can help prevent subsidence(20).

Interbody fusion devices

Over time, different materials have been used to make spinal cages, such as stainless steel (SS), ceramic, titanium, and polyetheretherketone (PEEK), with ongoing research into new ideal materials. The central aspect involved in developing implants for LIF is searching for a material that could be strong enough to withstand the loads applied to the spine and yet have an elastic modulus similar to bone(5). Materials should be biocompatible and promote osteoconductivity(21).

Currently, PEEK and titanium remain the most commonly utilized materials (Figure 3). Titanium has several advantages, including improved osteoconductive potential and resistance to corrosion, but with an elastic modulus of 110 GPa, it seems to be more prone to subsidence. Metal artifacts are also a concern during postoperative advanced image acquisition since they create a lot of distortion around the metal(5, 22).

On the other hand, PEEK has a smaller elastic modulus of around 4 GPa, being less prone to subsidence than titanium and closer to the bone elastic modulus (2.5 GPa). Also, PEEK is radiolucent, allowing a better assessment of fusion in the postoperative images. However, its surface is not osteoconductive, and bone integration is compromised. More recently, implants made of PEEK have been coated with a thin layer of titanium. The

thought is that the titanium coating would promote better bone integration; however, results have been inconclusive so far (5, 22).

Another feature that changes according to the LIF approach is the cage shape, size, and angles. The most common cage formats are mesh, cylindrical/bullet-shaped, rectangular/box-shaped, threaded, trapezoidal, and banana-shaped. Regardless of the shape, almost every implant has an open space to be filled with a morselized bone graft or synthetic grafts to facilitate fusion(5).



Figure 3. The picture shows 3 different types of cages. The first on the left, made of PEEK, the other two are made of titanium.

Among the cage shapes, the banana-shaped cage usually used during TLIF procedures is placed over the endplate's medial aspect, where the bone is generally weaker. Thus, it would be more prone to subsidence than straight-shaped cages that usually find their support on the periphery(5, 15, 18).

Biomechanical studies demonstrated that bigger cages could help to prevent subsidence and segmental stability(14). Still, massive cages used in ALIF and LLIF procedures are not

suitable for PLIF/TLIF procedures since the dissection corridor is smaller, with a higher risk of damage to neural structures(5).

More recently, concerns about the mismatch between cage sizes and angles available during ALIF and LLIF procedures led a group of surgeons to print custom-made titanium cages for patients according to preoperative scans and surgical planning(23).

Rapid prototyping

Rapid prototyping(RP) is a process involving the development of digital three-dimensional (3D) models that will be transformed into physical objects through additive manufacturing or 3D printing(3DP)(Figure 4)(24). Although available for a long time, its limited use in medicine, particularly in improving spine surgery, leaves ample opportunity for further exploration. The development of RP has provided the potential for personalized care for the patient, and the propagation of rapid prototyping has helped reduce the costs involved in the process. Also, surgical guides and orthosis can be developed and tailored to the patient's specific needs. Customized implants can help changing outcomes in complex surgeries since commercially available implants may not be suitable for significant or challenging reconstructions even with different standard sizes(25, 26). Moreover, it has been demonstrated that a patient-specific implant can reduce the risk of subsidence after a disc replacement surgery(27).

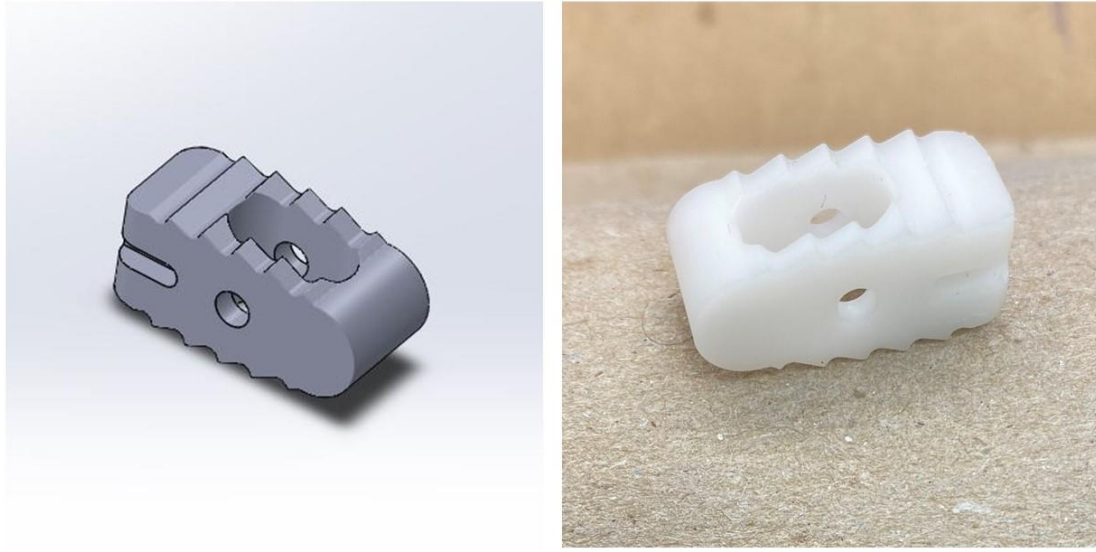


Figure 4. Cage 3D model developed using reverse engineering and its 3D printed aspect.

Novel research related to patient-specific interbody devices

An extensive literature review found only a few previous studies comparing interbody cages shapes and sizes demonstrating a significant reduction in endplate subsidence by increasing the surface of contact with larger devices(14, 15).

Despite the increased availability of rapid-prototyping techniques and the possibility of the development of patient-specific interbody fusion devices, only a few papers exploited this resource as a way to mitigate the risk of subsidence. de Beer et al. evaluated the reduction in the risk of subsidence during disc replacement surgeries. This type of surgery involves the complete removal of the intervertebral disc, including the annulus fibrosus, and the device usually rests on the periphery of the endplate(27), which helps avoid subsidence(20).

Other authors have studied conformational implants for LIF using Finite Element (FE) models created through Boolean subtractions from the endplate. Hence, they are expected to have a perfect match of the cross-sectional area between the digital 3D bone model and the digital 3D cage model. Also, these anteriorly inserted patient-specific implants created were bigger than the standard PLIF cages used during posterior approaches surgeries(22, 28, 29).

Posterior approaches have the smallest dissection windows for cage placement inside the disc space. Still, they remain the most performed techniques used for LIF(7), and subsidence appears to be among the most significant postoperative complications(30). To my knowledge, there has not been any investigation into whether patient-specific implants for PLIF cages can mitigate the risk of endplate subsidence.

Research goals

This study aims to investigate strategies to reduce the risk of subsidence when using PLIF implants. The primary strategy is to optimize the load distribution between the cage and bone endplate's contact surfaces. In order to accomplish this primary goal, two studies will be carried out.

1. The first study's objective is to investigate if the bone graft can improve mechanical loading support and help prevent subsidence. This role of the bone graft housed inside the cage has not been studied yet.
2. The second study will be carried out to investigate whether PLIF implants with matching bone interface geometry can reduce the risk of subsidence when compared to standard off-the-shelf implants with flat geometries used for a standard posterior

approach. This study has two objectives. For the first objective, we intend to investigate if the 3D printed patient-specific cages will indeed promote a bigger proportional surface of contact on the bone compared to commercial cages. And for the second objective, through a biomechanical study, we propose evaluating if the PLIF patient-specific implants that match the endplate bone geometry are superior in resistance to subsidence compared to two widely used commercial PLIF cages.

References

1. Kobayashi K, Ando K, Nishida Y, Ishiguro N, Imagama S. Epidemiological trends in spine surgery over 10 years in a multicenter database. *Eur Spine J.* 2018;27(8):1698-703.
2. de Kunder SL, Rijkers K, Caelers I, de Bie RA, Koehler PJ, van Santbrink H. Lumbar Interbody Fusion: A Historical Overview and a Future Perspective. *Spine (Phila Pa 1976).* 2018;43(16):1161-8.
3. Mobbs RJ, Phan K, Malham G, Seex K, Rao PJ. Lumbar interbody fusion: techniques, indications and comparison of interbody fusion options including PLIF, TLIF, MI-TLIF, OLIF/ATP, LLIF and ALIF. *J Spine Surg.* 2015;1(1):2-18.
4. Spiker WR, Goz V, Brodke DS. Lumbar Interbody Fusions for Degenerative Spondylolisthesis: Review of Techniques, Indications, and Outcomes. *Global Spine J.* 2019;9(1):77-84.
5. Patel DV, Yoo JS, Karmarkar SS, Lamoutte EH, Singh K. Interbody options in lumbar fusion. *J Spine Surg.* 2019;5(Suppl 1):S19-s24.
6. Formica M, Vallerga D, Zanirato A, Cavagnaro L, Basso M, Divano S, et al. Fusion rate and influence of surgery-related factors in lumbar interbody arthrodesis for degenerative spine diseases: a meta-analysis and systematic review. *Musculoskelet Surg.* 2020;104(1):1-15.
7. Goz V, Weinreb JH, Schwab F, Lafage V, Errico TJ. Comparison of complications, costs, and length of stay of three different lumbar interbody fusion techniques: an analysis of the Nationwide Inpatient Sample database. *Spine J.* 2014;14(9):2019-27.
8. Chang CW, Fu TS, Chen WJ, Chen CW, Lai PL, Chen SH. Management of Infected Transforaminal Lumbar Interbody Fusion Cage in Posterior Degenerative Lumbar Spine Surgery. *World Neurosurg.* 2019;126:e330-e41.
9. Urquhart JC, Collings D, Nutt L, Kuska L, Gurr KR, Siddiqi F, et al. The Effect of Prolonged Postoperative Antibiotic Administration on the Rate of Infection in Patients Undergoing Posterior Spinal Surgery Requiring a Closed-Suction Drain: A Randomized Controlled Trial. *J Bone Joint Surg Am.* 2019;101(19):1732-40.
10. Lee N, Kim KN, Yi S, Ha Y, Shin DA, Yoon DH, et al. Comparison of Outcomes of Anterior, Posterior, and Transforaminal Lumbar Interbody Fusion Surgery at a Single Lumbar Level with Degenerative Spinal Disease. *World Neurosurg.* 2017;101:216-26.
11. Macki M, Anand SK, Surapaneni A, Park P, Chang V. Subsidence Rates After Lateral Lumbar Interbody Fusion: A Systematic Review. *World Neurosurg.* 2019;122:599-606.
12. Oh KW, Lee JH, Lee JH, Lee DY, Shim HJ. The Correlation Between Cage Subsidence, Bone Mineral Density, and Clinical Results in Posterior Lumbar Interbody Fusion. *Clin Spine Surg.* 2017;30(6):E683-e9.
13. Zhou QS, Chen X, Xu L, Li S, Du CZ, Sun X, et al. Does Vertebral End Plate Morphology Affect Cage Subsidence After Transforaminal Lumbar Interbody Fusion? *World Neurosurg.* 2019;130:e694-e701.
14. Yuan W, Kaliya-Perumal AK, Chou SM, Oh JY. Does Lumbar Interbody Cage Size Influence Subsidence? A Biomechanical Study. *Spine (Phila Pa 1976).* 2020;45(2):88-95.
15. Tan JS, Bailey CS, Dvorak MF, Fisher CG, Oxland TR. Interbody device shape and size are important to strengthen the vertebra-implant interface. *Spine (Phila Pa 1976).* 2005;30(6):638-44.

16. Lakshmanan P, Purushothaman B, Dvorak V, Schrott W, Thambiraj S, Boszczyk M. Sagittal endplate morphology of the lower lumbar spine. *Eur Spine J.* 2012;21 Suppl 2(Suppl 2):S160-4.
17. Wang Y, Battié MC, Videman T. A morphological study of lumbar vertebral endplates: radiographic, visual and digital measurements. *Eur Spine J.* 2012;21(11):2316-23.
18. Grant JP, Oxland TR, Dvorak MF. Mapping the structural properties of the lumbosacral vertebral endplates. *Spine (Phila Pa 1976).* 2001;26(8):889-96.
19. Grant JP, Oxland TR, Dvorak MF, Fisher CG. The effects of bone density and disc degeneration on the structural property distributions in the lower lumbar vertebral endplates. *J Orthop Res.* 2002;20(5):1115-20.
20. Cadman J, Sutterlin C, 3rd, Dabirrahmani D, Appleyard R. The importance of loading the periphery of the vertebral endplate. *J Spine Surg.* 2016;2(3):178-84.
21. Jain S, Eltorai AE, Ruttiman R, Daniels AH. Advances in Spinal Interbody Cages. *Orthop Surg.* 2016;8(3):278-84.
22. Chatham LS, Patel VV, Yakacki CM, Dana Carpenter R. Interbody Spacer Material Properties and Design Conformity for Reducing Subsidence During Lumbar Interbody Fusion. *J Biomech Eng.* 2017;139(5):0510051-8.
23. Tartara F, Bongetta D, Pilloni G, Colombo EV, Giombelli E. Custom-made trabecular titanium implants for the treatment of lumbar degenerative discopathy via ALIF/XLIF techniques: rationale for use and preliminary results. *Eur Spine J.* 2020;29(2):314-20.
24. Popescu D, Laptioiu D. Rapid prototyping for patient-specific surgical orthopaedics guides: A systematic literature review. *Proc Inst Mech Eng H.* 2016;230(6):495-515.
25. Gadia A, Shah K, Nene A. Emergence of Three-Dimensional Printing Technology and Its Utility in Spine Surgery. *Asian Spine J.* 2018;12(2):365-71.
26. Wilcox B, Mobbs RJ, Wu AM, Phan K. Systematic review of 3D printing in spinal surgery: the current state of play. *J Spine Surg.* 2017;3(3):433-43.
27. de Beer N, Scheffer C. Reducing subsidence risk by using rapid manufactured patient-specific intervertebral disc implants. *Spine J.* 2012;22(11):1060-6.
28. Patel RR. Does patient-specific implant design reduce subsidence risk in lumbar interbody fusion? A bottom up analysis of methods to reduce vertebral endplate stress. Denver, CO: University of Colorado Denver; 2018.
29. Zhang M, Pu F, Xu L, Zhang L, Liang H, Li D, et al. development of an integrated CAD-FEA system for patient-specific design of spinal cages. *Comput Methods Biomech Biomed Engin.* 2017;20(4):355-64.
30. Chrastil J, Patel AA. Complications associated with posterior and transforaminal lumbar interbody fusion. *J Am Acad Orthop Surg.* 2012;20(5):283-91.

Chapter 2 - Biomechanical evaluation of morselized bone graft for preventing interbody fusion device subsidence.

Introduction/Background

The rate of instrumented spinal fusion procedures has increased over the last decades(1), and the use of interbody fusion devices (IFD) to achieve this is well established both in the cervical and the lumbar spine(2, 3). IFD can be made of different materials (e.g., titanium, PEEK) and in different shapes and sizes. In addition to promoting the goal of fusion, an IFD is intended to help maintain foraminal height and correct sagittal or coronal alignment(4).

Implant subsidence is an ongoing concern for interbody fusion. The subsidence of the device through one or both adjacent vertebral endplates can result in pseudoarthrosis, deterioration in alignment, and loss of the desired effect of indirect decompression of the neural elements. Subsidence rates are reported between 2-83%(2) for the cervical spine and 7-38% for the lumbar spine(5, 6).

Several risk factors of cage subsidence have been reported, including osteoporosis, cage materials, shape and size, and morphology of the endplate(7-10). To prevent implant subsidence, the vertebra-device interface's strength must surpass the applied loads(7).

To attenuate the risk of subsidence, strategies, such as loading the peripheral rim of the endplate(11), increasing the cage size(10), or creating patient-specific cages(12) to improve the surface of contact between the IFD and the endplate, have been employed. Most cages present an open space to house morselized bone grafts or synthetic bone substitutes to

increase fusion rates(13). To our knowledge, there is no published study so far exploring the graft's biomechanical contribution to preventing subsidence.

Thus, we proposed to: (I) investigate the role of morselized bone graft packed within the IFD into the prevention of IFD subsidence; and (II) determine if the compression force used to pack the morselized bone graft influences mechanical support to minimize cage subsidence.

Methodology

The methodology was based on previously published biomechanical studies on spine testing that used similar preparation methods(10, 14). A static axial compressive load was applied as recommended by ASTM standards for measuring load-induced subsidence of intervertebral body fusion devices(15).

Materials

Bone graft: After institutional Research Ethics Board (REB) approval, vertebrae bones were obtained from donated cadavers. The posterior elements were removed from thawed fresh frozen cadavers and morselized first using a rongeur followed by a bone mill to an approximate size of 2 mm, to mimic what is done in the operating room. Bone graft was kept moist during all the testing.

Simulated vertebral bodies: To standardize testing, cellular rigid polyurethane foam blocks were used in lieu of cadaveric vertebral bodies (Sawbones, PacificResearch

Laboratories, Inc., Washington). The foam blocks had a density of 0.2g/cm³ and a compressive modulus of 47.5 MPa. Each test specimen had a dimension of 40 (length) x 40 (width) x 40 (height) mm.

Interbody fusion device: To reduce the variables and only assess the effect of loading bone graft, it was chosen to use only one type of commercially available titanium mesh cage with thin walls, with an outer diameter of 15.88mm (total area: 198mm² and the graft area: 121.5 mm²) for testing.

Methods

Four groups were defined for axial compressive testing. The first was the control group (CG), for which empty IFDs without graft were tested. The second group comprised of IFDs which contained hand-packed graft (HG). Using an electromechanical testing machine (Instron® 5967, Norwood, MA, USA), in the third group, the graft was packed into the IFD using 100N force (PG1) and in the fourth group, the graft was packed using 800N force (PG2). A custom-made bone graft impactor was designed and printed using additive manufacturing (Figure 1).

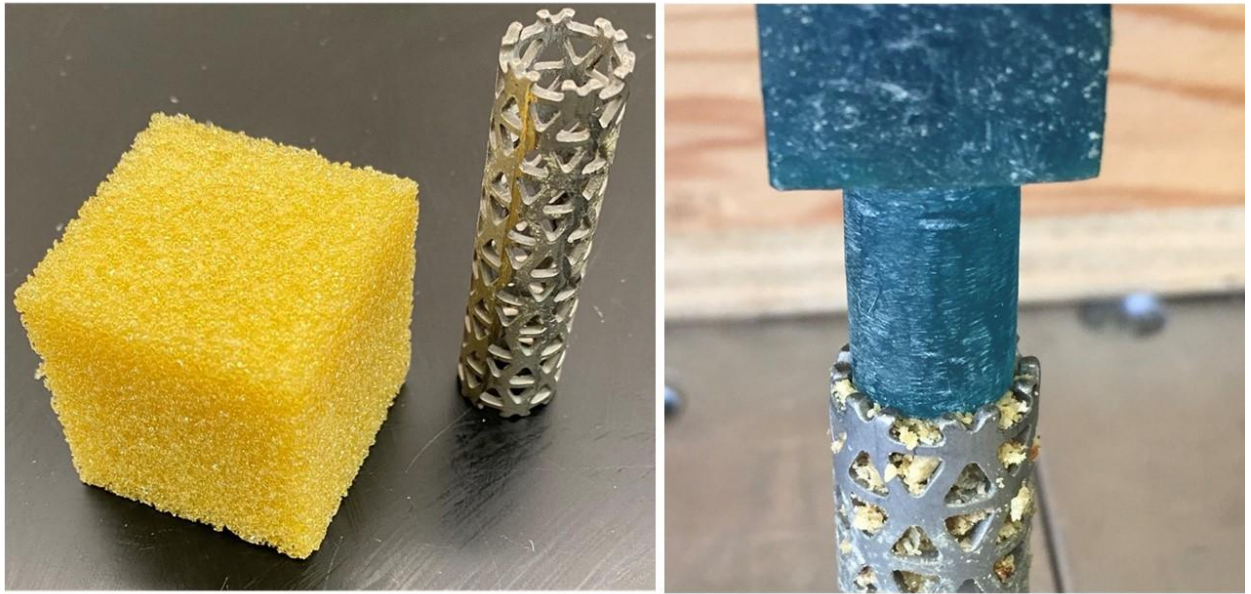


Figure 1. Left: Cage used for graft packing and a piece of synthetic bone used for testing. Right: customized bone impactor and the graft being compressed inside the cage.

Sample Size and testing order

Sixteen polyurethane foam blocks per group were used for testing, which is similar to previously published papers on spine biomechanical testing and more than ASTM(15) recommendations for in-vitro testing. The samples were placed in a list randomizer and were tested in the order provided by the computer.

Mechanical Compression Testing

The cage was compressed in the axial direction into the foam blocks at a rate of 0.1 mm/s(15) using an electromechanical testing machine (Instron® 5967, Norwood, MA, USA) until 10mm displacement was obtained. A 5N pre-load was applied before starting the test to ensure the testing head was in contact with the cage. A custom jig was printed using additive manufacturing to be placed on the top of the cage and ensure the proper alignment between the cage foam block. The tester's dedicated software recorded axial compressive force and displacement at a speed of 50Hz. Load, in Newtons, and construct stiffness (in N/mm) were extracted from the load-displacement curves.

Outcome variables

Failure force

In the clinical setting, subsidence was defined as relevant when a 3mm or more displacement occurs(16). Therefore, the mean force required for a 3 mm subsidence was compared among all the constructs.

Stiffness

Stiffness is the slope of the linear portion of the load-displacement curve plotted based on the data recorded from the tester's dedicated software. The initial linear part of the curve was selected, and a scatter plot was obtained. The first 0.5 millimetres of displacement was discarded to remove any possible accommodation artifacts. For all the

chosen segments, R^2 was higher than 0.98. Stiffness was obtained for all individual curves, and then the mean stiffness among the constructs was compared.

Statistical analysis

All statistical analyses were conducted using IBM SPSS version 26 (IBM Corp., Armonk, New York, USA). The mean constructs stiffness and mean failure load for each group were calculated. Comparisons between the failure force and stiffness were made using the Kruskal-Wallis test. When needed, the post-hoc Mann-Whitney U test was used to compare the possible combinations. Statistical significance was set at $p < 0.05$.

Results

Failure force

Failure force was 0.182 ± 0.02 in the CG, 0.181 ± 0.01 in the HG, 0.241 ± 0.03 in the PG1, and 0.314 ± 0.04 in the PG2. As more force was applied to compact the bone graft into the cage, significantly more force was required to produce a 3mm subsidence (Table 1). Post-hoc analysis showed a statistically significant difference between all paired groups except between CG and HG.

Stiffness

Stiffness (mean±SD) was 0.597±0.04 in the CG, 0.588±0.04 in the HG, 0.751±0.09 in the PG1, and 0.888±0.07 in the PG2. In the post-hoc analysis, the average stiffness was statistically different between all paired groups except CG and HG. Figure 2 shows the force-displacement curves for all the specimens, and figure 3 shows the mean force-displacement curves.

Table 1. Summary of results

Outcome	Group	N	Mean	Std. Deviation	Kruskal-Wallis test	Mann-Whitney U test		
						CG	HG	PG1
Force at 3mm (kN)	CG	16	0.597	0.038	<0.001			
	HG	16	0.588	0.040		0.651		
	PG1	16	0.751	0.089		<0.001	<0.001	
	PG2	16	0.888	0.068		<0.001	<0.001	<0.001
Stiffness (N/mm)	CG	16	0.182	0.022	<0.001			
	HG	16	0.181	0.013		0.970		
	PG1	16	0.241	0.032		<0.001	<0.001	
	PG2	16	0.314	0.043		<0.001	<0.001	<0.001

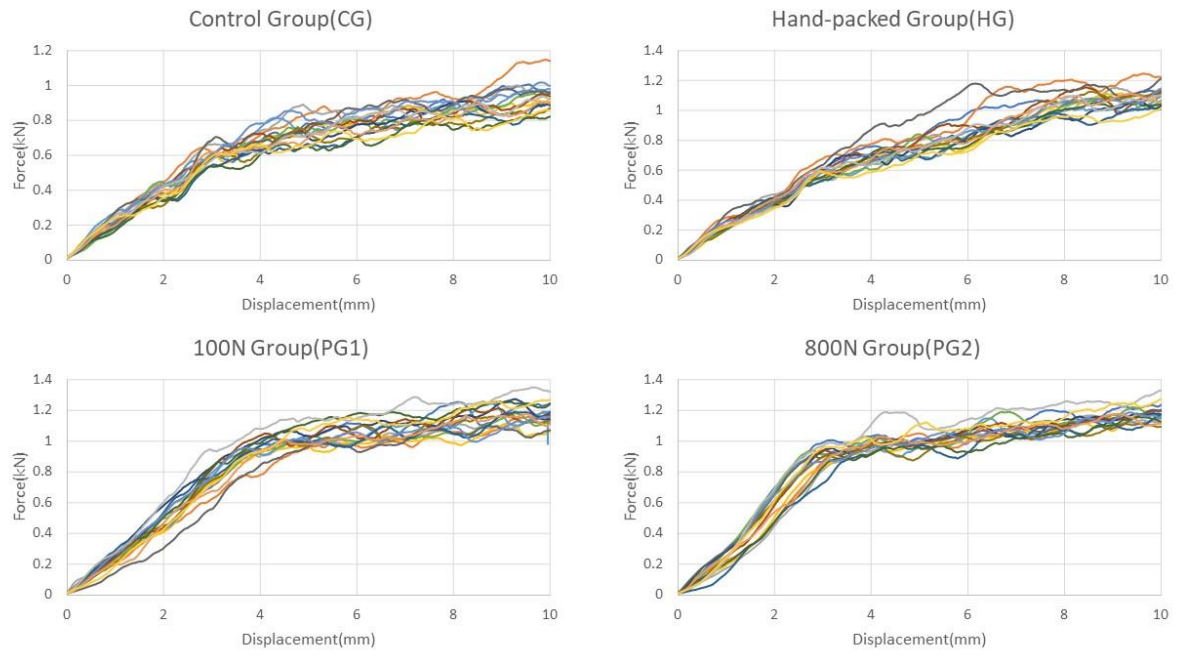


Figure 2. Force x displacement plots for every group.

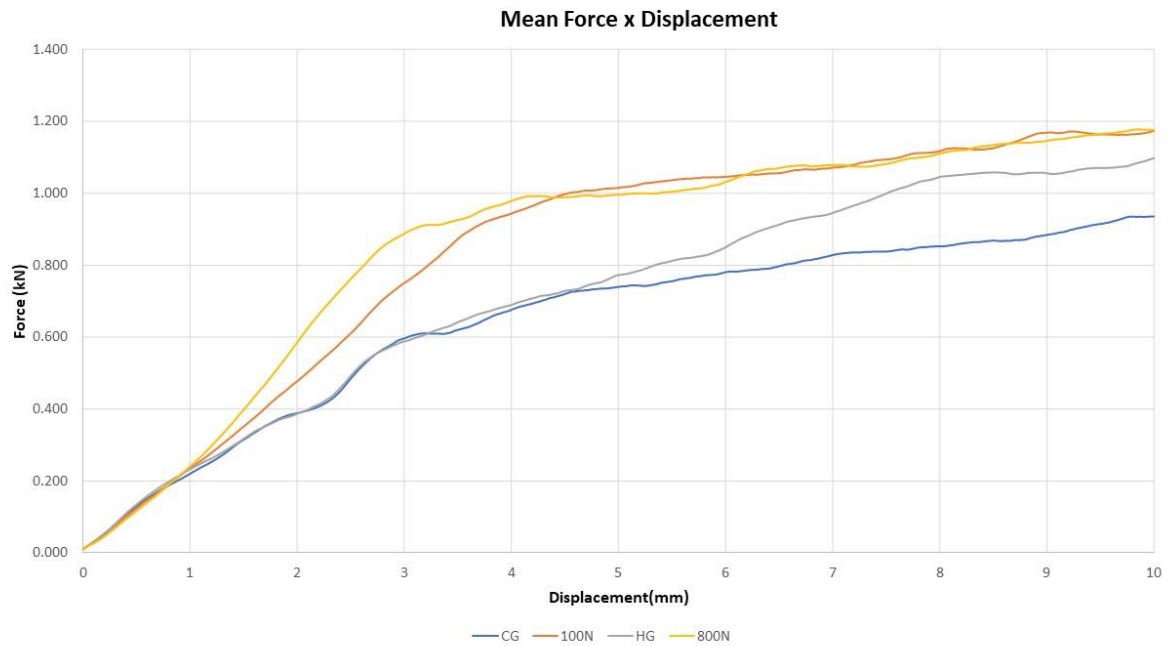


Figure 3. Mean force-displacement plot for the testing groups.

Discussion

This study finding's demonstrated that the bone graft's adequate compression within the IFD increases the force required for the occurrence of subsidence and increases the stiffness of the construct. The study compared the graft placed inside the IFD using manual compression and provided biomechanical evidence that it can be used more efficiently during IF procedures to reduce subsidence risk. This benefit is directly explained by the fact that the bone graft increases the load distribution area along with the cage surface, thus providing more mechanical support. Our study used what is considered clinically relevant subsidence (3mm) as one of the outcomes(16).

Interbody fusion has been used to treat spinal disorders for many years(3), and subsidence remains one of the most critical complications(17). Different IFD sizes are available for implantation during interbody fusion procedures, but bigger approaches are necessary to increase its width. It was shown in a study that larger cages were biomechanically superior in relation to smaller-sized cages(10). Still, they cannot be used at every spine level due to approach limitations(18). Since most of the IFD commercialized have an open space to house bone graft, the packing of this space with a morselized bone graft can be used as an ally to reduce the risk of subsidence. The cage used in this study had a graft area of 121.5 mm², corresponding to 61% of the cage's total area (198mm²). We anticipate that the differing proportion of graft area to the total implant contact area between commercially available IFDs will have a varying magnitude of effect; however, this was not directly tested in this study.

As the compression load used to pack bone inside the cage increased, so did the construct stiffness. Compressing the bone graft increases the bone graft elastic modulus bringing it closer to the cortical bone elastic modulus. Thereby, it causes the stress to redistribute from the implant to the graft site, leading to better transmission of load through the construct and an increased synthetic bone-construct interface strength. In addition to the potential advantage in limiting subsidence, Lee et al.(19) reported less than 50% of bone growth inside the cage related to the stress-shielding effect negatively affecting the bone ingrowth due to rigid titanium constructs. Also, bone fusion rates increase when the graft is kept under compression(20).

We obtained our bone graft from posterior elements of lumbar spines and used a bone mill to morselize the bone in the same fashion it is done during spinal surgery. Although our graft was kept moist during the testing, Fosse et al.(21) showed in their study that different amounts of fat and water could interfere with the stiffness of the morselized bone graft. It has also been demonstrated that the graft grain size may affect the construct's mechanical stability(22). Still, we did not control for this variable to reproduce the conditions during surgical procedure faithfully.

Rigid polyurethane foam blocks were used for this study since they allow standardizing the testing. They have a similar density to human bone mimicking cancellous bone and were validated for testing IFD subsidence(14). They help to avoid the bone density variability intrinsic to cadaveric bones. Still, they do not show a sharp deflection point while breaking the endplate's cortical bone shell when looking at the force-displacement plot. Another advantage of using foam blocks is that they have a flat surface allowing the cage to sit flat on the top during the biomechanical testing instead of the typical irregular surface of the human endplate(23) and thus removing possible peak stress areas.

This study has its limitations. First, it is an in-vitro biomechanical test studying constant compressive forces in one direction. It does not consider the full range of motion and shear forces to which a human spine is subjected. The graft compression was limited to the point where the graft started to leak out of the cage through the holes in the mesh; therefore, cages with a closed graft placement area would possibly increase the compression force. Also, we used an electromechanical testing machine to compress the graft to a high force, not available in the surgical environment. Furthermore, although foam blocks are validated for biomechanical testing, they do not replicate the thin cortical layer in the endplate and the differences in bone density across the vertebral body, but they allow less variability in the results of biomechanical testing.

Conclusion

Our results bring new proof of concept about the importance of densely packing the bone graft inside the IFD. It plays an essential role in reducing the risk of cage subsidence.

References

1. de Kunder SL, Rijkers K, Caelers I, de Bie RA, Koehler PJ, van Santbrink H. Lumbar Interbody Fusion: A Historical Overview and a Future Perspective. *Spine (Phila Pa 1976)*. 2018;43(16):1161-8.
2. Noordhoek I, Koning MT, Jacobs WCH, Vleggeert-Lankamp CLA. Incidence and clinical relevance of cage subsidence in anterior cervical discectomy and fusion: a systematic review. *Acta Neurochirurgica*. 2018;160(4):873-80.
3. Patel DV, Yoo JS, Karmarkar SS, Lamoutte EH, Singh K. Interbody options in lumbar fusion. *J Spine Surg*. 2019;5(Suppl 1):S19-s24.
4. Champagne PO, Walsh C, Diabira J, Plante ME, Wang Z, Boubez G, et al. Sagittal Balance Correction Following Lumbar Interbody Fusion: A Comparison of the Three Approaches. *Asian Spine J*. 2019;13(3):450-8.
5. Macki M, Anand SK, Surapaneni A, Park P, Chang V. Subsidence Rates After Lateral Lumbar Interbody Fusion: A Systematic Review. *World Neurosurg*. 2019;122:599-606.
6. Rao PJ, Phan K, Giang G, Maharaj MM, Phan S, Mobbs RJ. Subsidence following anterior lumbar interbody fusion (ALIF): a prospective study. *J Spine Surg*. 2017;3(2):168-75.
7. Tan JS, Bailey CS, Dvorak MF, Fisher CG, Oxland TR. Interbody device shape and size are important to strengthen the vertebra-implant interface. *Spine (Phila Pa 1976)*. 2005;30(6):638-44.
8. Park MK, Kim KT, Bang WS, Cho DC, Sung JK, Lee YS, et al. Risk factors for cage migration and cage retropulsion following transforaminal lumbar interbody fusion. *Spine J*. 2019;19(3):437-47.
9. Zhou QS, Chen X, Xu L, Li S, Du CZ, Sun X, et al. Does Vertebral End Plate Morphology Affect Cage Subsidence After Transforaminal Lumbar Interbody Fusion? *World Neurosurg*. 2019;130:e694-e701.
10. Yuan W, Kaliya-Perumal AK, Chou SM, Oh JY. Does Lumbar Interbody Cage Size Influence Subsidence? A Biomechanical Study. *Spine (Phila Pa 1976)*. 2020;45(2):88-95.
11. Cadman J, Sutterlin C, 3rd, Dabirrahmani D, Appleyard R. The importance of loading the periphery of the vertebral endplate. *J Spine Surg*. 2016;2(3):178-84.
12. de Beer N, Scheffer C. Reducing subsidence risk by using rapid manufactured patient-specific intervertebral disc implants. *Spine J*. 2012;12(11):1060-6.
13. Ba Z, Zhao W, Wu D, Shen B, Yu B, Wang Z. Box cages packed with local decompression bone were efficient in anterior cervical discectomy and fusion: five- to 10-year follow-up. *Spine (Phila Pa 1976)*. 2012;37(20):E1260-3.
14. Au AG, Aiyangar AK, Anderson PA, Ploeg HL. A new bone surrogate model for testing interbody device subsidence. *Spine (Phila Pa 1976)*. 2011;36(16):1289-96.
15. ASTM F2267-04(2018), Standard Test Method for Measuring Load Induced Subsidence of Intervertebral Body Fusion Device Under Static Axial Compression, ASTM International, West Conshohocken, PA, 2018, www.astm.org.
16. Gercek E, Arlet V, Delisle J, Marchesi D. Subsidence of stand-alone cervical cages in anterior interbody fusion: warning. *Eur Spine J*. 2003;12(5):513-6.

17. Lee N, Kim KN, Yi S, Ha Y, Shin DA, Yoon DH, et al. Comparison of Outcomes of Anterior, Posterior, and Transforaminal Lumbar Interbody Fusion Surgery at a Single Lumbar Level with Degenerative Spinal Disease. *World Neurosurg.* 2017;101:216-26.
18. Mobbs RJ, Phan K, Malham G, Seex K, Rao PJ. Lumbar interbody fusion: techniques, indications and comparison of interbody fusion options including PLIF, TLIF, MI-TLIF, OLIF/ATP, LLIF and ALIF. *J Spine Surg.* 2015;1(1):2-18.
19. Lee JH, Jeon DW, Lee SJ, Chang BS, Lee CK. Fusion rates and subsidence of morselized local bone grafted in titanium cages in posterior lumbar interbody fusion using quantitative three-dimensional computed tomography scans. *Spine (Phila Pa 1976).* 2010;35(15):1460-5.
20. Bolger C, Bourlion M, Leroy X, Petit D, Vanacker G, McEvoy L, et al. Maintenance of graft compression in the adult cervical spine. *Eur Spine J.* 2006;15(8):1204-9.
21. Fosse L, Rønningen H, Benum P, Sandven RB. Influence of water and fat content on compressive stiffness properties of impacted morsellized bone: an experimental ex vivo study on bone pellets. *Acta Orthop.* 2006;77(1):15-22.
22. Putzer D, Coraça-Huber D, Wurm A, Schmoelz W, Nogler M. Optimizing the grain size distribution of allografts in bone impaction grafting. *J Orthop Res.* 2014;32(8):1024-9.
23. Wang Y, Battié MC, Videman T. A morphological study of lumbar vertebral endplates: radiographic, visual and digital measurements. *Eur Spine J.* 2012;21(11):2316-23.

Chapter 3 – Biomechanical evaluation of the amount of congruent bone endplate and 3d printed patient-specific PLIF cage vs commercial cage.

Introduction

Lumbar interbody fusion (LIF) has been widely used to treat different pathologies in the lumbar spine, including degenerative scoliosis, spinal stenosis, and degenerative disc disease, but several complications have been described(1, 2).

Among the complications, implant subsidence remains the most common challenge to overcome. Subsidence is defined when the cage penetrates one or both adjacent vertebral bodies' endplates, and it can cause loss of segmental lordosis, relapse of foraminal compression, and pain(3).

Several strategies can be used to help reduce the incidence of subsidence, including the use of different materials (e.g., polyetheretherketone (PEEK) vs. titanium), alternative surgical approaches allowing placement of bigger cages, and increasing the total area of contact between the cage and the vertebral body endplate(4-6).

Rapid prototyping (RP) is among the options to increase the contact area between the interbody fusion device and the endplate. It is a process that allows the development of a three-dimensional (3D) customized implant matching the patient's endplate bone anatomy, thus increasing the contact area when compared to commercially available implants(7). This strategy can play a critical role in posterior approaches using posterior LIF(PLIF) cages since the small dissection window limits their size for placement inside the disc space.

Some papers have studied the effectiveness of conformational implants for LIF using Finite Element (FE) models(8-10). These models are created through a Boolean subtraction of the endplate; hence they are expected to have a perfect match of the cross-sectional area between the digital 3D bone model and the digital 3D cage model.

However, the settings used in the clinic computed tomography (CT) scans protocol may pose limitations to the customized implant model. CT-scan spatial resolution is determined by multiple parameters (e.g., collimation, pitch)(11). Digitally the implant and bone model may match, but if the bone model used to create the implant was not created using sufficient resolution, there would be a mismatch in the resulting implant and real bone surface.

Also, another limitation of the development process of a patient-specific device is the 3D printer used. The laser beam spot size and the layer thickness can influence the final resolution of the 3D printed device(12).

Although intuitively, a patient-specific design should result in a higher area of contact, due to differences in resolution, this may not be the case. There is a lack of evidence in the literature that confirms a patient-specific cage's effectiveness in creating a greater contact area.

In the present study, we use a cadaveric model to investigate the possible mismatch in 3D printed patient-specific cages with the endplate and compare their performance to commercially available cages.

Methodology

Anatomical specimens acquisition

Five full spine cadavers samples were purchased through United Tissue Network, a donor organization that provides cadavers for medical research and education. The specimens were received with non-identifiable information regarding their medical history, cause of death, gender, and age. Before use, cadaveric samples were stored in a -20°C freezer.

CT-Scan

After institutional Research Ethics Board approval, the full spine cadaveric specimens were subject to CT-Scan to rule out bone tumours or fractures and to obtain image acquisition for the segmentation process. The soft tissues remained intact during the scanning process to replicate the clinical scenario as much as possible. The spines were scanned using a GE Lightspeed VCT 64 slice CT Scanner with 0.625mm slice thickness. The scanning protocol was the same used for clinical lumbar spine protocol in our institution. It uses the following parameters: Pitch 0.984:1, table speed 39.37mm/ro, Helical Full 1.0s, SFOV: Large Body, DFOV 40 adjust as needed, 120 kVp, Auto mA: ON Smart mA: ON, Min mA: 200 Max mA: 650, Dose Reduction: 20%, Noise Index: 26 and ASIR: 40%.

Bone cleaning process

The spines were isolated from L1 to L5 and prepared in a similar way, as described in previous studies(13). Most of the muscles were resected, and the bones were submerged in water for 3 hours with dishwashing detergent to make the process of cleaning more

efficient. This procedure helped the breakdown of fats and the detachment of remaining tissues. After the process, the specimens were carefully cleaned not to damage the bones inadvertently. A combination of gentle sharp dissection using a scalpel, curettes, and periosteal elevators were used to remove soft tissue. Special care was taken during the cartilaginous endplate removal to avoid damage to the underlying bony endplate. After removing all the soft tissue, the bones dried at room temperature. After the bones were dry, they were potted in cement with the cranial endplate parallel to the ground (Figure 1).



Figure 5. L5 vertebra potted in cement for biomechanical testing.

Sample size

Four vertebrae were excluded from the 25 dissected lumbar vertebrae because they had been damaged during the cadaver harvesting process. Another three vertebra were excluded, one due to a previous fracture, another due to the presence of Schmorl's nodes and a third one was damaged during initial Fujifilm range selection testing. Therefore, 18 vertebrae were available for testing. They were then balanced in two groups of 9 vertebrae each, and each group was assigned to a comparison group (patient-specific vs. Capstone

and patient-specific vs. Fuse). Each vertebra's left and the right side was tested for both the patient-specific cage and the commercial cage allowing 18 samples per comparison group.

Bone segmentation

An open-source software, 3D Slicer (version 4.10.2), was used to create 3D mesh models by importing the CT digital imaging and communication in medicine (DICOM) files.

A region of interest was created around each superior endplate for every lumbar vertebral body (L1-L5), using the data from the 0.625mm slice thickness bone reconstructions, with a spacing scale of 0.7 and isotropic spacing. Cropping the region of interest helped to reduce the amount of data in the image and improved computer processing times. Each endplate model was created using manual segmentation by the 'grow from seeds' extension in the Segment Editor of 3D Slicer (Figure 2). Bone and soft-tissue were extracted based on different Hounsfield Units (HU). Segmentation defects were corrected by modifying seeds when needed, with care taken to compare the final segmentation model to the original CT-scan reconstruction. Closing (fill holes) smoothing effect at a kernel size of 0.6 mm was used to obtain a final model, which was exported as an STL file. The CT scan models were designated as endplate models.

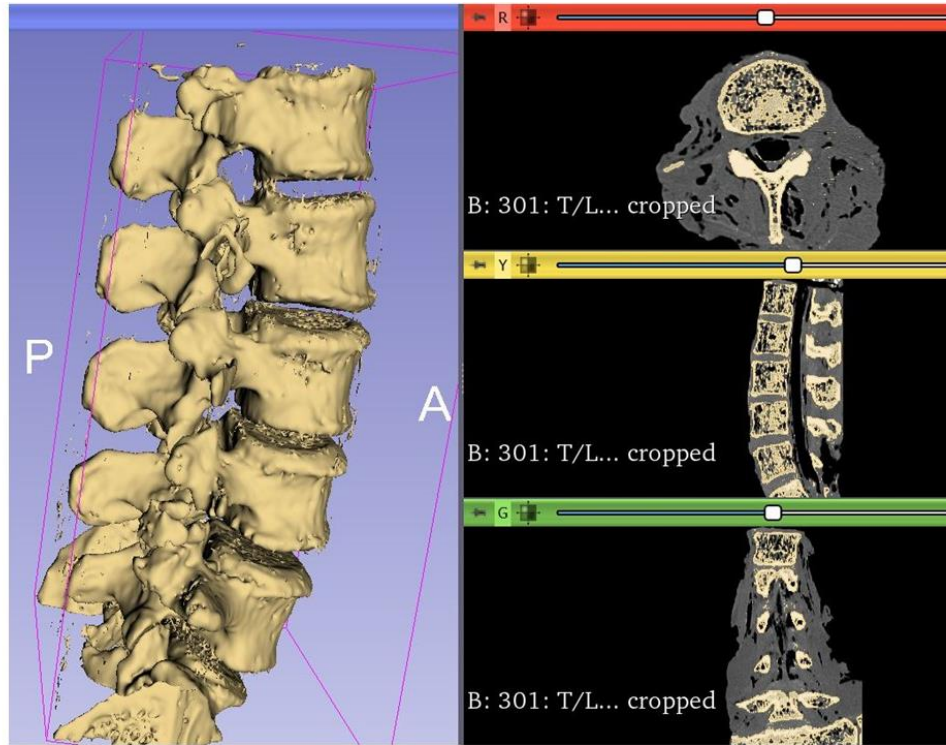


Figure 6. Example of 3D segmentation of the lumbar spine using 3D Slicer. Each vertebra file was saved as an individual file.

Choice of commercially available PLIF cage models

Although several different types and cages brands are available for PLIF spinal surgery, their shapes can be summarized into two major types: cylindrical/bullet-shaped cages and rectangular/box-shaped cages(14). Therefore, we decided to use two types of commercially available intervertebral PLIF cages provided by a single prominent medical device company supplier (Medtronic Sofamor Danek USA, Inc., Memphis, TN, USA). One was made out of titanium alloy and had a cylindrical shape (FUSE™ Spinal System); the other was made out of PEEK and had a rectangular shape (CAPSTONE® PEEK Spinal

System) (Figure 3). Both cages are hollow, allowing the bone graft to be packed inside the device. Both implants had the same width (10mm) and length (22mm).

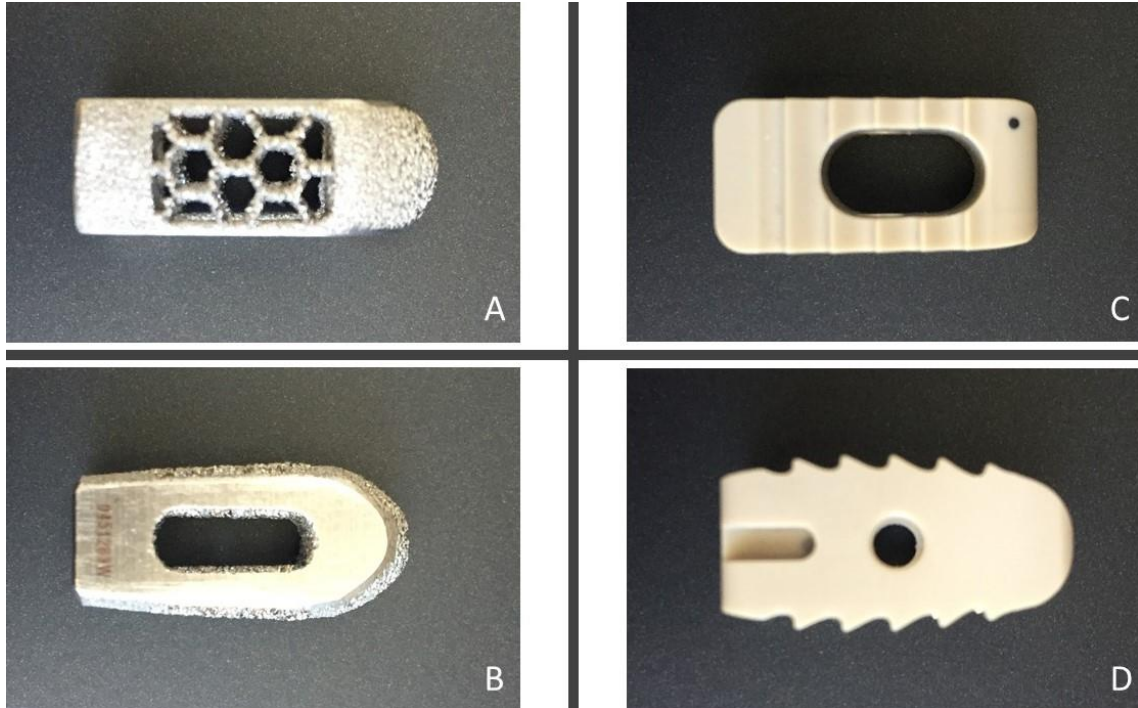


Figure 7. Superior and lateral views of FUSE™ cage (A-B) and CAPSTONE® cage(C-D).

Cage design

Reverse engineering processes were used to replicate the dimensions and features of the cages. A digital calliper (Igaging EzCal), with 0.01mm resolution, was used to make manual measurements of the cages and their dimensions. Pictures were taken to be used as blueprints during the design process. The modified implant models for subsidence testing were designed in CAD 3D modelling software (SolidWorks 2019, Dassault Systèmes Solidworks Corp.). They were initially designed as a full implant and then cut in half to

allow the addition of a base of support to enable the implant to be attached to the testing machine (Figure 4). After the process was concluded, the cylindrical cage model and the rectangular cage model corresponding files were exported as an STL file.

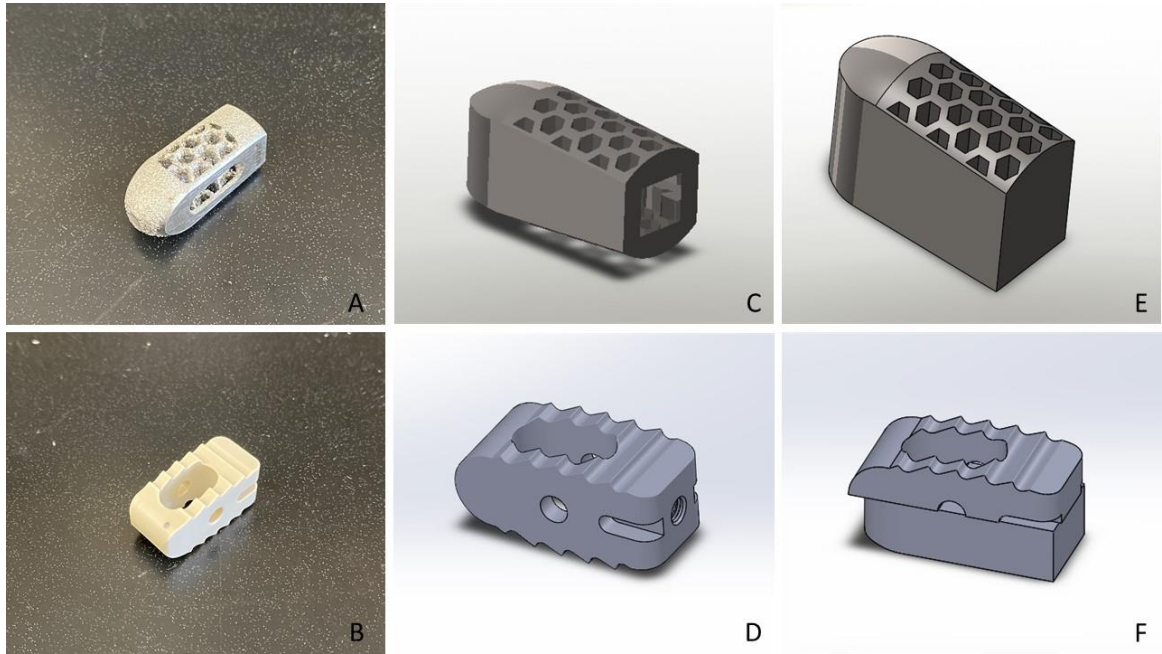


Figure 8. Images showing pictures of the original Fuse and Capstone cages (A, B), their full implant CAD models (C, D), and the CAD models used for the biomechanical testing (E, G).

Patient-specific cages design

The superior endplate models and the cylindrical cage model were imported into a STL editing software (Netfabb, Autodesk Inc, San Rafael, California). Two Fuse PLIF implants (left and right) were translated for every endplate until their geometry was overlapping with each vertebra's superior endplate in a similar position it would be placed

during a PLIF surgery procedure (Figure 5). After that, a Boolean subtraction operation was performed to create two patient-specific PLIF cages per vertebra. Also, a guide for each endplate was designed to place the cages in the correct position during testing (Figure 6). Every patient-specific cage and endplate guide was exported as an STL file.

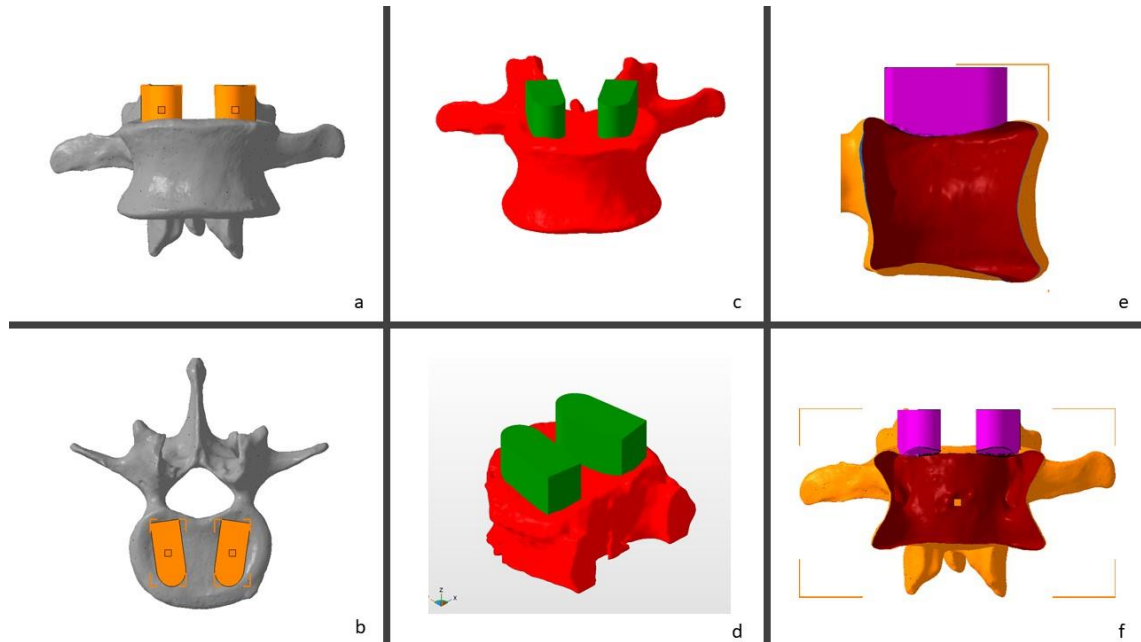


Figure 9. Anterior and superior views of cage planned positions(a-b), anterior and oblique views of the Boolean operation(c-d), and lateral and anterior views of the hollow vertebra and the conformational implant post-Boolean operation(e-f).

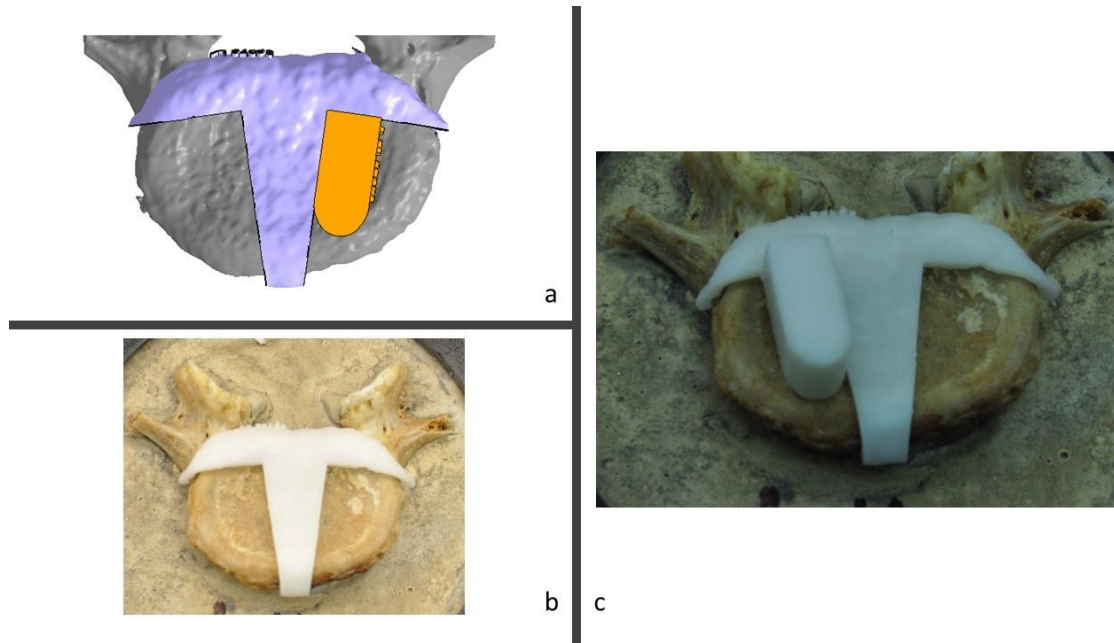


Figure 10. a-c: Guide created to help placement of the custom cage in the right position.

Cage 3D printing

All the STL files, including the endplate guide, the patient-specific cages, and the modified cylindrical and rectangular-shaped cages, were imported into the FormLabs PreForm software to be printed using a Form 2 printer (FormLabs, Somerville, Massachusetts). The models were oriented on the build platform to avoid placing supports on parts of the cages that would contact the endplate during testing. The layer thickness was set to 50 microns to improve resolution. Since our goal was to evaluate the cages' shape, all the models were printed in Rigid resin (FormLabs, Somerville, Massachusetts) to standardize the material. This resin is reinforced with glass fibre making it resistant to deformation and has an Elastic Modulus similar to PEEK.

Pressure-sensitive Fujifilm

Different methods are used to evaluate the interface between medical devices and joints or bones(15). Pressure-sensitive measurement film (Fujifilm, Pressure Metrics, Whitehouse Station, NJ, USA) is one method to measure contact areas and contact pressure. It consists of two sheets containing active coating on one side. When both sides containing active coating are compressed together against each other, red stains are released from the translucent sheet over the opaque white sheet. The more intense the stain, the higher the pressure applied over the area. Different types of pressure-sensitive films are available, and they encompass different ranges of pressure (Table 1).

Table 2. Fujifilm pressure ranges (Pressure Metrics, Whitehouse Station, NJ, USA)

Pressure Film Type	Code	Pressure Range
Ultra Extreme Low	5LW	0.87 - 7.3 PSI (0.06 - 0.51 kg/cm ²)
Extreme Low	LLLLW / 4LW	7.2 - 28 PSI (0.5 - 2 kg/cm ²)
Ultra Super Low	LLLW	28 - 87 PSI (2 - 6 kg/cm ²)
Super Low	LLW	70 - 350 PSI (5 - 25 kg/cm ²)
Low	LW	350 - 1,400 PSI (25 - 100 kg/cm ²)
Medium	MS	1,400 - 7,100 PSI (100 - 500 kg/cm ²)
High	HS	7,100 - 18,500 PSI (500 - 1,300 kg/cm ²)
Super High	HHS	18,500 - 43,200 PSI (1,300 - 3,000 kg/cm ²)

Testing set-up

Pressure-sensitive measurement film ("Ultra super low" Fujifilm, Pressure Metrics, Whitehouse Station, NJ, USA) was inserted at the interface of each cage-vertebra construct. It had a 0.2mm thickness, with a minimum 0.19MPa (i.e., 28 psi) and a maximum 0.6 MPa (i.e., 87 psi) pressure sensing threshold. The sheets were cut into 30mm × 30mm squares. After determining each ideal cage position, the Fujifilm indicator layer was placed on the top of the endplate and the acid layer above the indicator layer (Figure 7). Using an electromechanical testing machine (Instron® 5967, Norwood, MA, USA), the cages were compressed axially over the vertebra's endplate with a 100 Newtons(N) force for 30 seconds to obtain a consistent stain. The 100N force was chosen to avoid damage to the endplate. A higher force could cause the endplate surface geometry to change. All cages were packed with bone graft to replicate similar conditions in surgery. Finally, after every test, the endplate surface was thoroughly inspected to assess any surface conditioning that could interfere with the next test.

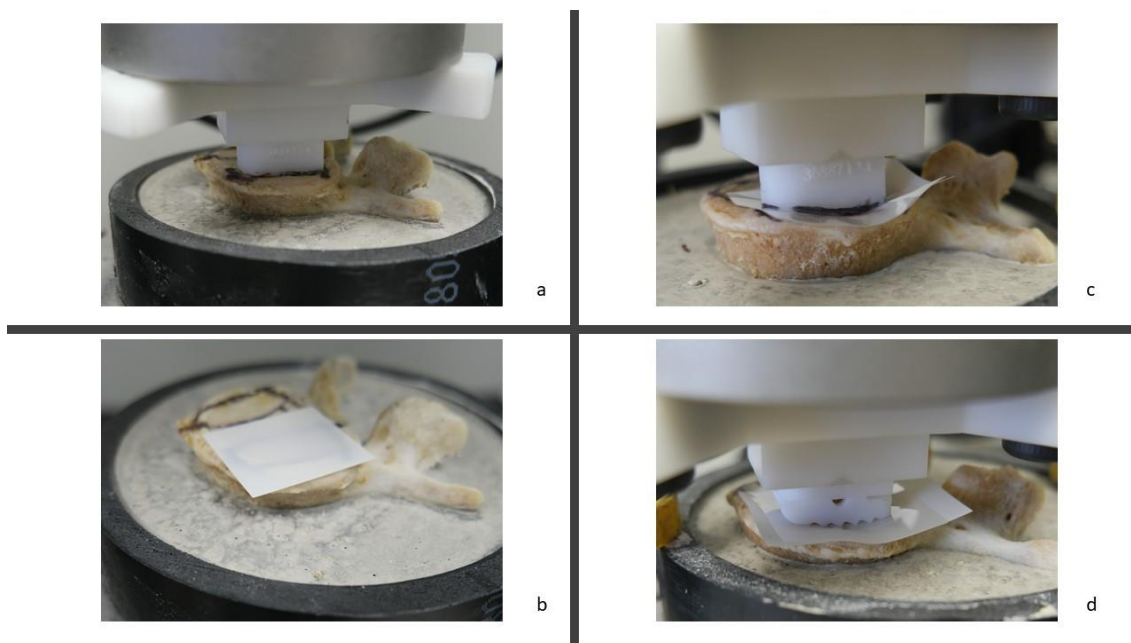


Figure 11. (a) Ideal cage position was determined using PS cage, (b) FujiFilm was put in place, (c-d) PS and commercial cage being compressed over the FujiFilm.

Contact area and contact stress analysis

After the load was removed, Fujifilm sheets were carefully removed from the top of the endplate. Afterward, the Fujifilm indicator layers' contact areas were scanned in jpeg format at 1200 dpi (dots per inch) using a desktop scanner (Hewlett-Packard, HP ENVY 4520). The maximum contact area of the cages that were touching the endplates was calculated using the ImageJ software (version 1.52, U. S. National Institutes of Health, Bethesda, Maryland, USA). On the software, the red-coloured images of the cage's contact area were converted from RGB to HSB 8-bit images, allowing the colours to be converted to grayscale, such that we obtained a white image of the cage's contact area on a dark background. A histogram was obtained, and its values were recorded in a datasheet. To properly calibrate the thresholding limits, an object with a known area was compressed over the Fujifilm. Then, the threshold limits were set in a way that at least 95% of the area was reached (Appendix A). Thus, every cage's histogram was used to obtain the cage contact area measured in mm². Mean contact stress was obtained by dividing the applied force (100N) by the measured contact area and was reported in megapascals (MPa). Also, a separate analysis for each cage was done according to the vertebral level to assess if there were differences in effectiveness according to the depth of the endplate.

Statistical analysis

After obtaining the contact area and the mean contact stress for every cage tested, two comparison groups were created: patient-specific vs. rectangular cage (Capstone) and patient-specific vs. cylindrical cage (Fuse). Comparison between groups was made using a two-tailed paired *t*-test. Also, for every cage, ANOVA was used to compare the mean contact area per lumbar spinal vertebra. Statistical significance was set at $p < 0.05$.

Results

Cage contact area

In group 1, in which the PS cage was compared to the Capstone cage, the mean contact area obtained was $100 \pm 23.6 \text{ mm}^2$ and $57.5 \pm 13.7 \text{ mm}^2$ for PS and Capstone cages, respectively. In group 2, the PS cage was compared to the Fuse cage, and the mean contact area was $104.8 \pm 39.6 \text{ mm}^2$ and $55.2 \pm 35.1 \text{ mm}^2$, respectively. For both groups, the PS mean contact area was significantly different than the Capstone and Fuse cages contact areas ($p < 0.0001$) (Table 2).

A subgroup analysis per cage, per spine vertebra, showed no difference when comparing the mean contact area among the different levels ($p > 0.05$) (Table 3).

Contact stress

In group 1, the Capstone cage mean contact-stress was 73% higher than the PS cage ($1.84 \text{ vs. } 1.06 \text{ MPa}$, $p < 0.0001$), while in group 2, the Fuse cage mean contact stress was 122% higher than the PS cage ($2.44 \text{ vs. } 1.10 \text{ MPa}$, $p < 0.0001$).

Contact footprint Vs Total Surface Area

Each cage had a maximum possible contact area of 220mm². Results from Fujifilm analysis show that PS cages combined had an average contact footprint of 46.5% of the total area (mean=102.4mm²). The Capstone and Fuse cages had a contact footprint of 26.1% and 25.1% of the total possible area, respectively (Figure 8).

Table 3. Mean±SD cage contact areas, in mm², and contact stress, in megapascals (MPa).

	Cage	N	Mean	Std. Deviation	p-value
Contact area					
Group 1	PS	18	100.0	23.6	<0.0001
	Capstone	18	57.5	13.7	
Group 2	PS	18	104.8	39.6	<0.0001
	Fuse	18	55.2	35.1	
Contact stress					
Group 1	PS	18	1.06	0.28	<0.0001
	Capstone	18	1.84	0.45	
Group 2	PS	18	1.10	0.43	<0.0001
	Fuse	18	2.44	1.32	

Table 4. Mean±SD contact area subgroup analysis per cage per level (in mm²).

Level	N	Mean	Std. Deviation	Test	p-value
Patient-Specific Cage					
L1	6	114.1	50.7	ANOVA	0.716
L2	8	100.9	34.0		
L3	6	96.2	34.1		
L4	8	109.8	23.6		
L5	8	92.4	21.7		
Fuse Cage					
L1	2	81.0	42.2	Welch ANOVA	0.090
L2	4	38.6	7.7		
L3	4	87.6	50.1		
L4	4	51.7	24.0		
L5	4	30.1	13.1		
Capstone Cage					
L1	4	51.1	14.7	ANOVA	0.824
L2	4	61.4	21.1		
L3	2	52.4	9.7		
L4	4	59.7	11.3		
L5	4	60.4	11.8		

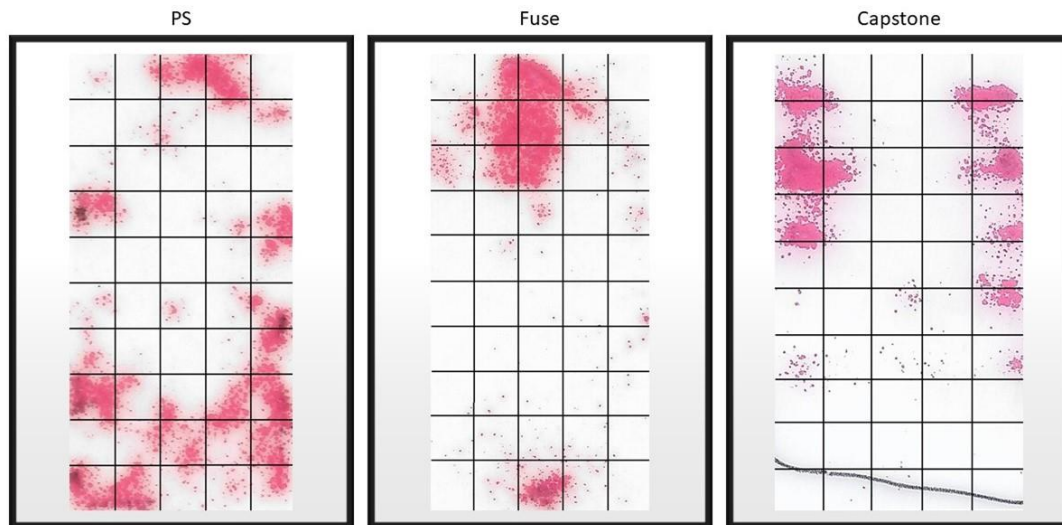


Figure 12. Sample imaging of the contact area for each of the cages.

Discussion

This study found that PLIF patient-specific cages increased in up to 73.9% the contact area between the cage and the endplate compared to commercially available PLIF cages. It resulted in better utilization of the cage's total area with better load sharing across the endplate and, therefore, resulted in significantly lower contact stress.

A biomechanical study(6) showed that by increasing the cage's size, the force required for subsidence increases due to a larger contact area, but they found out that when the length of PLIF cages was increased, it didn't increase substantially the force required for subsidence. It was attributed to the cage shape.

Analyzing contact area and pressure is essential to understand medical devices' biomechanical behaviour and their interaction with the human bone. Knowledge of this interaction can provide metrics to aid in improving future medical device design. When it comes to developing patient-specific interbody fusion devices, studies have explored finite element models to evaluate stress distribution across the endplate(8-10). They found that devices matching the endplate surface anatomy promote a reduction in the endplate stresses and subsidence risk. Due to the natural concave shape of the endplate, Patel(9) showed that for non-conformational implants, high-stress concentrations were located at the edges of the endplate-device interface, supporting our findings for the commercial cages' contact analysis. Also, Wang et al.(16) found that the cranial endplate depth was more significant at the lower lumbar spine levels than the upper lumbar vertebrae. Still, it did not favour any of the cages in our level-by-level analysis (Table 3).

In contrast to a finite element patient-specific implant that reaches a perfect match to the endplate contour, our 3D printed patient-specific cages did not have the same

effectiveness. None of the tested PS cages resulted in staining 100% of the cage area during the Fujifilm compression test. However, results were still significantly larger than the commercial cages stain area. The lack of a complete match between the cage and the endplate is likely related to the CT scan's limitations. Image quality is determined by choice of image parameters(11). In this study, to evaluate the mismatch between the cage developed by the CT 3D vertebra reconstruction, a typical clinical lumbar spine image acquisition protocol was used. Kanawati et al. (17) compared 3D CT-based vertebrae models to 3D scanned cadaveric bones and found an excellent geometric overlap between models. Still, the CT 3D model had a significantly higher volume than the bone volume showing a mismatch between the CT image and the bone size. No studies were found during the literature review investigating the possible differences between the endplate CT image resolution and the bony endplate contour.

Nonetheless, there are limitations in this study. First, pressure-sensitive films are widely used for orthopedic biomechanics research, but they have several limitations related to handling, image processing, temperature and moisture sensitivity, and pressure thresholding(15). For this study, an "Ultra super low" Fujifilm was used, and the pressure range was from 0.19 to 0.6MPa. Since the force applied to the cages was limited to 100N to avoid damage to the endplate during testing, the total contact area can be underestimated since the minimum threshold may not have been reached in some contact points. At the same time, folds on the film during the test can generate false-positive areas of contact. Also, during the image processing, the stain's intensity was not evaluated to differentiate higher pressure regions. It was only reported as the presence or absence of contact.

Secondly, this is an in-vitro cadaveric study; therefore, the meticulous process involved in cleaning the endplate may not be reproduced in-vivo during surgery and can create distortions in the final endplate aspect.

Moreover, the 3D printing process itself can add errors to the cage's final aspect since the mere change in the device orientation in the printing platform can cause distortions related to the resin curing process. FormLabs Rigid resin was used to print all the cages in this study because it has an Elastic Modulus similar to PEEK's Elastic Modulus being resistant to deformation when subjected to high forces and more practical for laboratory tests. Also, guides were created to help place the cages in the ideal position during testing, but this would not be possible in the clinical scenario due to the guide's size; alternatives like intra-operative navigation would be used instead.

Despite the limitations mentioned above, the present study proposed investigating whether small 3D printed patient-specific devices, such as PLIF cages, reflect an increase in the contact area similar to that described by the computational models of endplate and implant contact. The study demonstrated the presence of a mismatch between the CT-based 3D vertebra model and the real endplate anatomy. Still, PLIF patient-specific cages can achieve a larger contact area compared to one-size-fits-all commercially available cages.

Conclusion

Patient-specific cages can maximize the contact area between the implant and the endplate surface, reducing the contact stress and the risk of implant subsidence during PLIF surgeries.

References

1. Mobbs RJ, Phan K, Malham G, Seex K, Rao PJ. Lumbar interbody fusion: techniques, indications and comparison of interbody fusion options including PLIF, TLIF, MI-TLIF, OLIF/ATP, LLIF and ALIF. *J Spine Surg.* 2015;1(1):2-18.
2. Spiker WR, Goz V, Brodke DS. Lumbar Interbody Fusions for Degenerative Spondylolisthesis: Review of Techniques, Indications, and Outcomes. *Global Spine J.* 2019;9(1):77-84.
3. Lee N, Kim KN, Yi S, Ha Y, Shin DA, Yoon DH, et al. Comparison of Outcomes of Anterior, Posterior, and Transforaminal Lumbar Interbody Fusion Surgery at a Single Lumbar Level with Degenerative Spinal Disease. *World Neurosurg.* 2017;101:216-26.
4. Patel DV, Yoo JS, Karmarkar SS, Lamoutte EH, Singh K. Interbody options in lumbar fusion. *J Spine Surg.* 2019;5(Suppl 1):S19-s24.
5. Wang Y, Lu T, He X, Wen Z, Gao Z, Gao Z, et al. Effect of Dome-Shaped Titanium Mesh Cages on Cervical Endplate Under Cyclic Loading: An In Vitro Biomechanics Study. *Med Sci Monit.* 2019;25:142-9.
6. Yuan W, Kaliya-Perumal AK, Chou SM, Oh JY. Does Lumbar Interbody Cage Size Influence Subsidence? A Biomechanical Study. *Spine (Phila Pa 1976).* 2020;45(2):88-95.
7. Popescu D, Laptoiu D. Rapid prototyping for patient-specific surgical orthopaedics guides: A systematic literature review. *Proc Inst Mech Eng H.* 2016;230(6):495-515.
8. Chatham LS, Patel VV, Yakacki CM, Dana Carpenter R. Interbody Spacer Material Properties and Design Conformity for Reducing Subsidence During Lumbar Interbody Fusion. *J Biomech Eng.* 2017;139(5):0510051-8.
9. Patel RR. Does patient-specific implant design reduce subsidence risk in lumbar interbody fusion? A bottom up analysis of methods to reduce vertebral endplate stress. Denver, CO: University of Colorado Denver; 2018.
10. Zhang M, Pu F, Xu L, Zhang L, Liang H, Li D, et al. Development of an integrated CAD-FEA system for patient-specific design of spinal cages. *Comput Methods Biomech Biomed Engin.* 2017;20(4):355-64.
11. Tins B. Technical aspects of CT imaging of the spine. *Insights Imaging.* 2010;1(5-6):349-59.
12. Calignano F, Galati M, Iuliano L, Minetola P. Design of Additively Manufactured Structures for Biomedical Applications: A Review of the Additive Manufacturing Processes Applied to the Biomedical Sector. *J Healthc Eng.* 2019;2019:9748212.
13. Galvez M, Montoya CE, Fuentes J, Rojas GM, Asahi T, Currie W, et al. Error Measurement Between Anatomical Porcine Spine, CT Images, and 3D Printing. *Acad Radiol.* 2020;27(5):651-60.
14. Goh JC, Wong HK, Thambyah A, Yu CS. Influence of PLIF cage size on lumbar spine stability. *Spine (Phila Pa 1976).* 2000;25(1):35-9; discussion 40.
15. Sarwar A, Srivastava S, Chu C, Machin A, Schemitsch EH, Bougherara H, et al. Biomechanical Measurement Error Can Be Caused by Fujifilm Thickness: A Theoretical, Experimental, and Computational Analysis. *Biomed Res Int.* 2017;2017:4310314.
16. Wang Y, Battié MC, Videman T. A morphological study of lumbar vertebral endplates: radiographic, visual and digital measurements. *Eur Spine J.* 2012;21(11):2316-23.

17. Kanawati A, Fernandes RJR, Gee A, Urquhart J, Siddiqi F, Gurr K, et al. Geometric and Volumetric Relationship Between Human Lumbar Vertebra and CT-based Models. Acad Radiol. 2020.

Chapter 4 – Biomechanical comparison of subsidence between patient-specific and non-patient-specific PLIF cages.

Introduction

Lumbar interbody fusion (LIF) surgery is performed to treat different spine pathologies, and the indication for its use has been refined with the emergence of better evidence(1). With varying types of interbody fusion devices (IFD), LIF has improved fusion rates, helped correct deformities, improve coronal and sagittal balance, and establish mechanical stability(2, 3). The added advantage of LIF surgery is that it also restores the disc space height, thus directly and indirectly decompressing neural elements(4).

However, implant subsidence remains a significant concern after LIF. Subsidence occurs when the cage penetrates one or both adjacent vertebral bodies' endplates, and the reported occurrence rates range from 7% to 38%(5). After subsidence, the clinical outcomes can worsen, resulting in increased pain and loss of the desired effect of indirect decompression of the neural elements(6). Smaller IFD sizes used for posterior LIF (PLIF) surgeries have been correlated to an increased risk of implant subsidence(7).

Thanks to improvements in medical imaging and 3D image acquisition and processing, among strategies to reduce subsidence risk is the use of conformational implants matching the patient's bone and endplate shape(8). Finite element cage models have shown a decrease in stress distribution across the cage and the endplate by matching the endplate shape(9-11). Still, finite element models are idealized shapes and expected to have a perfect match to the 3D endplate cross-section area, which likely is not generalizable to the real-life clinical situation.

Rapid prototyping, or three-dimensional printing(3DP), is a manufacturing process with increasing applications to spine surgery(8, 12). It allows the printing of 3D objects from 3D models, layer by layer. Various objects have been produced and used in spine surgery to achieve specific objectives, including case reports using patient-specific (PS) cages for LIF surgery. Although PS cages have already been used in a clinical scenario(8), there is a possible mismatch between the final implant surface and the patient's endplate. The mismatch is related to image acquisition modalities(13) and the limitations in 3DP layers resolution(14). There is a lack of evidence in the literature that confirms the biomechanical superiority of 3D printed patient-specific PLIF cages in relation to commercially available cages.

In the present biomechanical study, we use a cadaveric model to investigate the resistance to subsidence in small PLIF patient-specific cages and compare their performance to commercially available cages.

Methodology

Anatomical specimens acquisition

Five full spine cadaveric samples were obtained through a donor organization (United Tissue Network) that provides cadavers for medical research and education. The specimens are received with non-identifiable information regarding their medical history, cause of death, gender, and age. The bone mineral density (BMD) was not known for the specimens in this study. Before use, cadaveric samples were stored in a -20°C freezer.

Lumbar spine CT-Scan image acquisition

After institutional Research Ethics Board (REB) approval, the full spine cadaveric specimens were subject to CT-Scan to obtain image acquisition for the segmentation process and to screen for bone tumours or fractures. The soft tissues were left intact during the imaging process. The specimens were scanned using a GE Lightspeed VCT 64 slice CT Scanner with 0.625mm slice thickness. The scanning protocol used followed typical settings for clinical imaging of the lumbar spine in our institution. It uses the following parameters: Pitch 0.984:1, table speed 39.37mm/ro, Helical Full 1.0s, SFOV: Large Body, DFOV 40 adjust as needed, 120 kVp, Auto mA: ON Smart mA: ON, Min mA: 200 Max mA: 650, Dose Reduction: 20%, Noise Index: 26 and ASIR: 40%.

Bone cleaning process

The spines were isolated from L1 to L5 and prepared in a similar way, as described in previous studies(15). Most of the muscles were resected. The bones were submerged in water for 3 hours with dishwashing detergent to make cleaning more efficient by helping break fats and detach the remaining tissues. After the process, the specimens were carefully cleaned not to damage the bones inadvertently. A combination of gentle sharp dissection using a scalpel and curette was used to remove soft tissue. Special care was taken during the cartilaginous endplate removal to avoid damage to the underlying bony endplate. After removing all the soft tissue, the bones dried at room temperature. After the bones were dry, they were potted in cement with the cranial endplate parallel to the ground (Figure 1).



Figure 13. L4 vertebra potted in cement for biomechanical testing.

Sample size

Four vertebrae were excluded from the 25 dissected lumbar vertebrae because they had been damaged during the cadaver harvesting process. Another three vertebra were excluded being one due to a previous fracture, another due to the presence of Schmorl's nodes and a third one was damaged during initial testing. Therefore, 18 vertebrae were available for testing. They were then balanced in two groups of 9 vertebrae each, and each group was assigned to a comparison group (patient-specific vs. Capstone and patient-specific vs. Fuse). Each vertebra's left and the right side was tested for the patient-specific cage, on one side, and the commercial cage, on the contralateral side, allowing 9 samples per comparison group.

Bone segmentation

An open-source software, 3D Slicer (version 4.10.2), was used to create 3D mesh models by importing the CT digital imaging and communication in medicine (DICOM) files.

A region of interest was created around each superior endplate for every lumbar vertebral body (L1-L5), using the data from the 0.625mm slice thickness bone reconstructions, with a spacing scale of 0.7 and isotropic spacing. Cropping the region of interest helped to reduce the amount of data in the image and improved computer processing times. Each endplate model was created using manual segmentation by the 'grow from seeds' extension in the Segment Editor of 3D Slicer (Figure 2). Bone and soft-tissue were extracted based on different Hounsfield Units (HU). Segmentation defects were corrected by modifying seeds when needed, with care taken to compare the final segmentation model to the original CT-scan reconstruction. Closing (fill holes) smoothing effect at a kernel size of 0.6 mm was used to obtain a final model, which was exported as an STL file. The CT scan models were designated as endplate models.

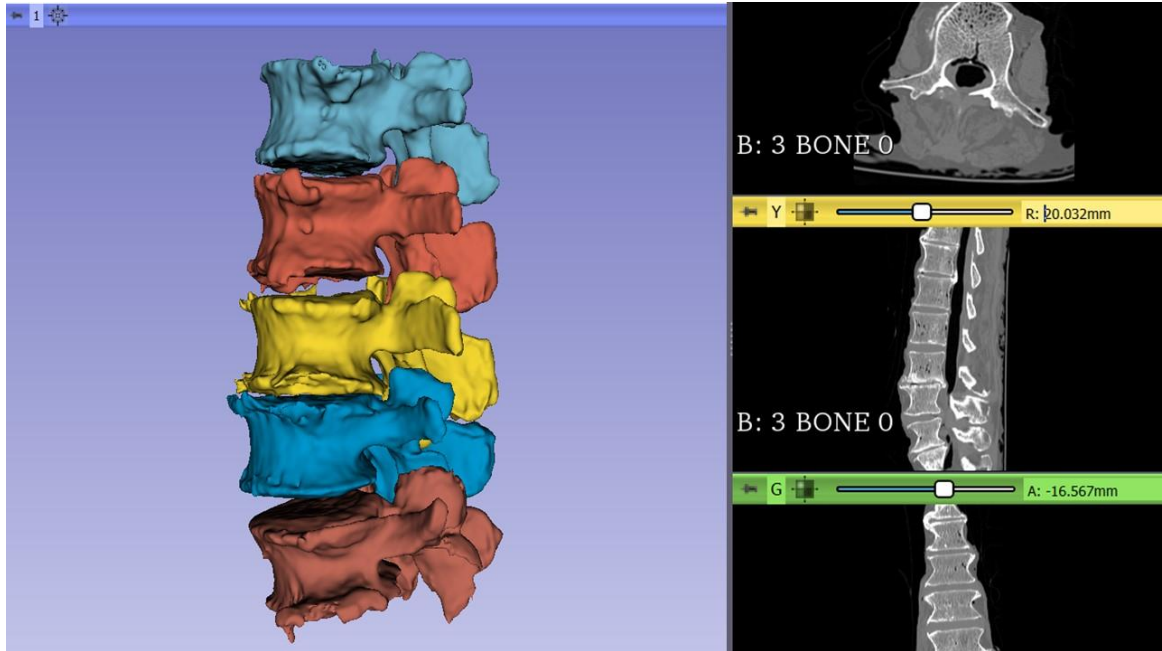


Figure 14. Example of individual vertebra segmentation of the lumbar spine using 3D Slicer. Each vertebra file was saved as a separate file.

Choice of commercially available PLIF cage models

Although several different types and cages brands are available for PLIF spinal surgery, their shapes can be summarized into two major types: cylindrical/bullet-shaped cages and rectangular/box-shaped cages(16). Therefore, we decided to use two types of commercially available intervertebral PLIF cages provided by a single prominent medical device company supplier (Medtronic Sofamor Danek USA, Inc., Memphis, TN, USA). One was made out of titanium alloy and had a cylindrical shape (FUSE™ Spinal System); the other was made out of polyetheretherketone (PEEK) and had a rectangular shape (CAPSTONE® PEEK Spinal System) (Figure 3). Both cages are hollow, allowing the bone

graft to be packed inside the device. Both implants had the same width (10mm) and length (22mm).

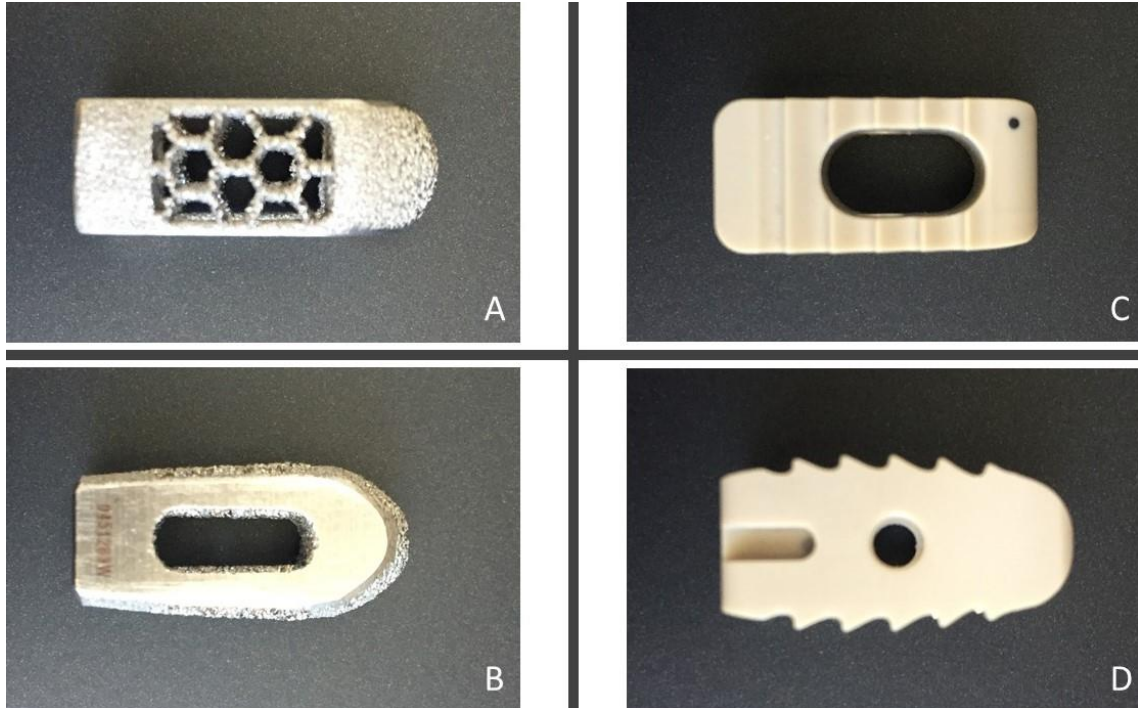


Figure 15. *FUSE® cage superior(A) and lateral(B) views and CAPSTONE® cage superior(C) and lateral views (D).*

Cage design

The dimensions and features of the cages were replicated digitally in CAD 3D modelling software (SolidWorks 2019, Dassault Systèmes Solidworks Corp.). A digital calliper (Igaging EzCal), with 0.01mm resolution, was used to make manual measurements of the cages and their dimensions. Photos were taken to be used as blueprints during the design process. The modified implant models for subsidence testing were designed in CAD

3D modelling software. They were initially designed as a full implant and then cut in half and modified to allow the addition of a base. This base enabled the implant to be attached to the testing machine (Figure 4). The cylindrical cage and rectangular cage models were exported as an STL file.

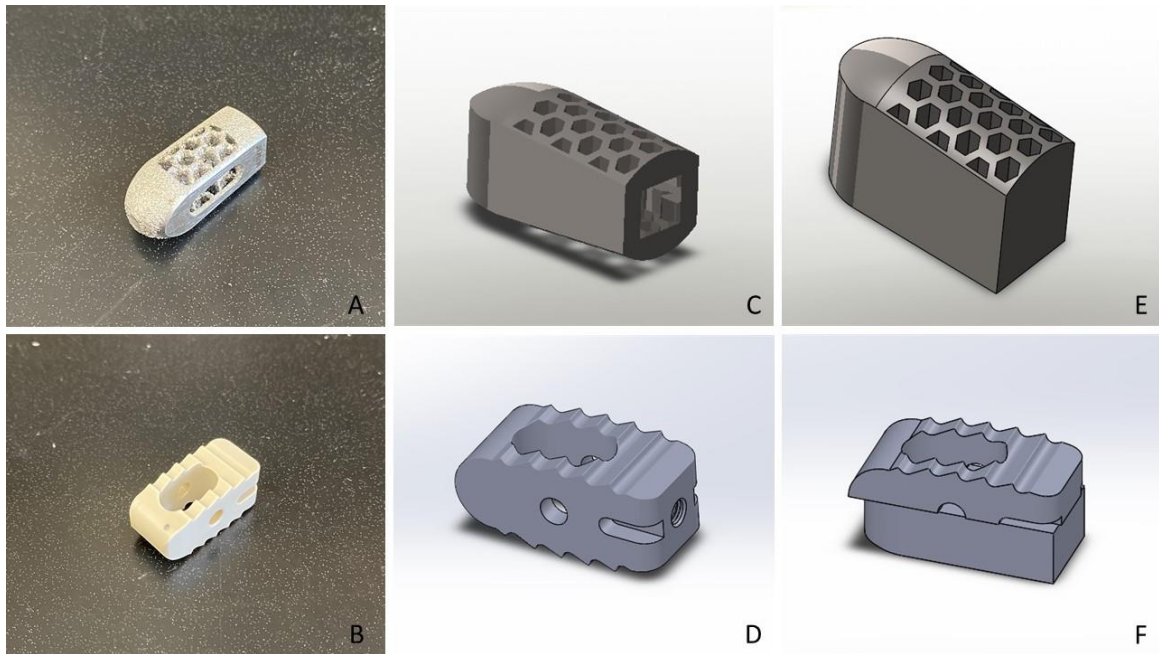


Figure 16. Images showing pictures of the original Fuse and Capstone cages (A, B), their full implant CAD models (C, D), and the CAD models used for the biomechanical testing (F, G).

Patient-specific cages design

The superior endplate models and the cylindrical cage model were imported into an STL editing software (Netfabb, Autodesk Inc, San Rafael, California). Two Fuse PLIF implants (left and right) were translated for every endplate until their geometry was overlapping with each vertebra's superior endplate in a similar position it would be placed

during a PLIF surgery procedure (Figure 5). After that, a Boolean subtraction operation was performed to create two patient-specific PLIF cages per vertebra. Also, a positioning guide for each endplate was designed to place the cages in the pre-planned position during testing (Figure 6). Every patient-specific cage and endplate guide was exported as an STL file.

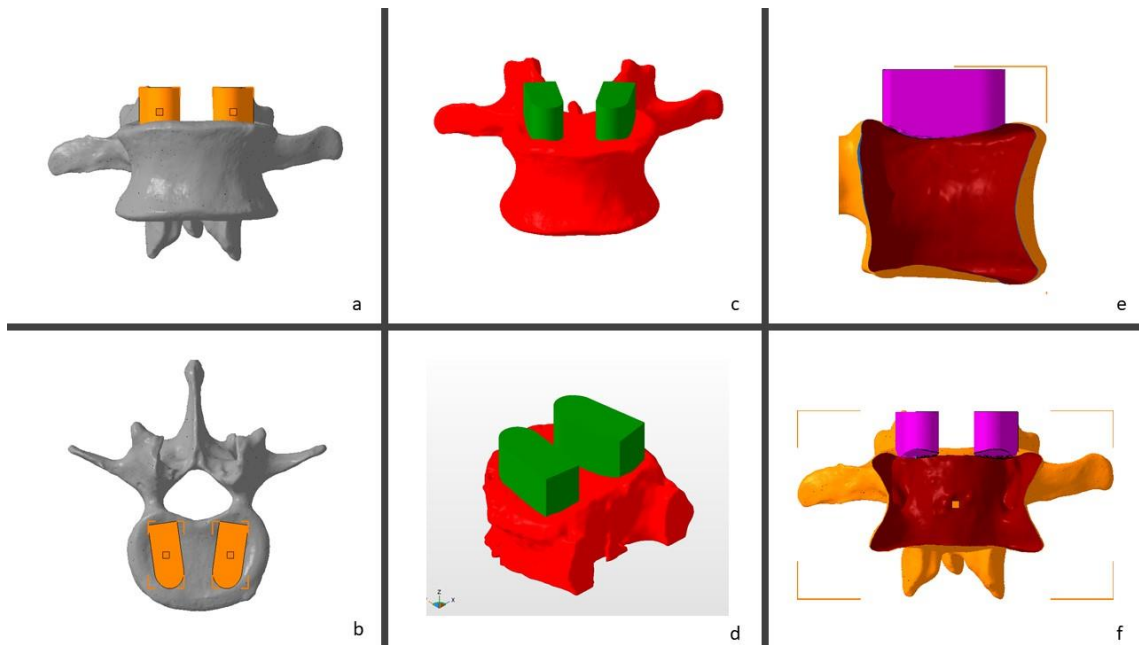


Figure 17. Anterior and superior views of cage planned positions(a-b), anterior and oblique views of the Boolean operation(c-d), and lateral and anterior views of the hollow vertebra and the conformational implant post-Boolean operation(e-f).

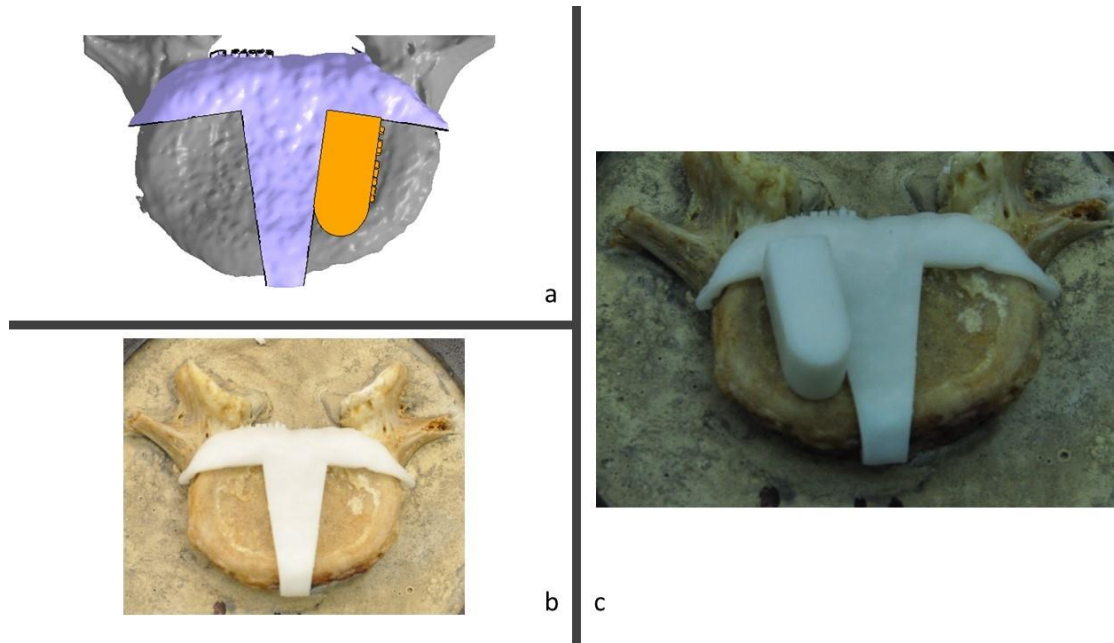


Figure 18. a-c: Guide created to help placement of the custom cage in the right position.

Cage 3D printing

All the STL files, including the endplate guide, the patient-specific cages, and the modified cylindrical and rectangular-shaped cages, were imported into the FormLabs PreForm software to be printed using Form 2 (FormLabs, Somerville, Massachusetts) printer. The models were oriented on the build platform to avoid placing supports on parts of the cages that would contact the endplate during testing. The layer thickness was set to 50 microns to improve resolution. Since our goal was to evaluate the cages' shape, all the models were printed in Rigid resin (FormLabs, Somerville, Massachusetts) to standardize the material. This resin is reinforced with glass fibre making it resistant to deformation and has an Elastic Modulus similar to PEEK.

Testing set-up

After determining each ideal cage position (Figure 7), half of the vertebrae (n=9) received a PS cage on the left side and a half on the right side alternately; therefore, one of the non-patient-specific PLIF cages was placed on the opposite side, and each specimen served as its own control. The cages were compressed axially over the vertebra's endplate at a rate of 0.1 mm/s(17) using an electromechanical testing machine (Instron® 5967, Norwood, MA, USA) until structural failure of the cage, vertebra, or both. To avoid material wear problems, none of the cages was tested twice. Axial compressive force and displacement were recorded automatically by the tester's dedicated software. Failure load (in Newtons, N) and construct stiffness (in N/mm) were extracted from the load-displacement curves. Failure load is the maximum load achieved in the load-displacement graph before the failure occurred, whereas stiffness is the slope of the linear portion of the load-displacement curve before a failure occurs.

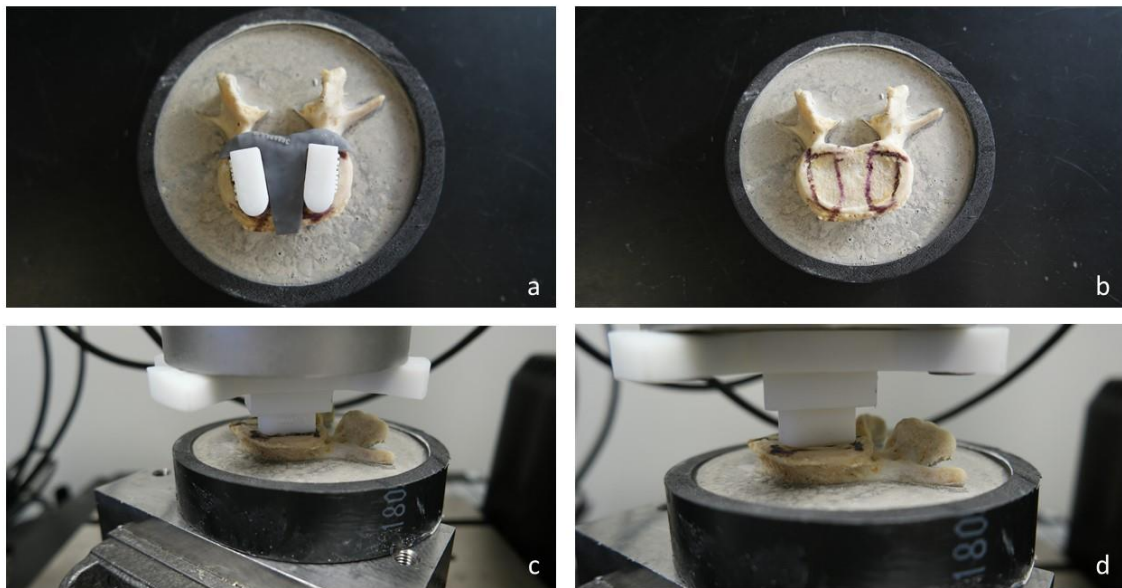


Figure 19. (a) Ideal cage position was determined endplate guide and cage, (b) positioning was recorded with marking pen, (c) PS cage was used to determine testing position, and commercial cage being placed in the same position for testing.

Statistical analysis

After obtaining the peak failure force and the stiffness for every cage tested, two comparison groups were created: patient-specific vs. rectangular cage (Capstone) and patient-specific vs. cylindrical cage (Fuse). Also, a separate analysis was done according to the vertebral level to assess if there were differences between the more cranial endplates (L1-L3) in relation to the more caudal lumbar endplates (L4-L5). Comparison between groups was made using a two-tailed paired *t*-test. Statistical significance was set at $p < 0.05$.

Results

Failure force

For the first group, where PS cages were compared to the Fuse cages, the failure force (mean \pm SD), in kN, was 1.399 ± 0.3 , for the PS cage, and 0.852 ± 0.2 , for the Fuse cage ($p < 0.001$) (Table 1).

For the second group, where PS cages were compared to Capstone cages, the failure force (mean \pm SD), in kN, was 1.381 ± 0.5 , for the PS cage, and 1.164 ± 0.5 , for the Capstone cage ($p = 0.086$) (Table 2).

Stiffness

For the first group, the stiffness (mean±SD), in kN/mm, was 1.275±0.2 for the PS cage, and 0.431±0.1, for the Fuse cage (p<0.001) (Table1).

For the second group, the stiffness (mean±SD), in kN/mm, was 1.382±0.5 for the PS cage, and 0.867±0.5, for the Capstone cage (p=0.009) (Table 2).

Table 5. Group 1 peak force and stiffness comparison between PS and Fuse cage with subgroup analysis for the upper lumbar spine(L1-L3) and lower lumbar spine (L4-L5).

Patient-Specific x Fuse Cage			
Peak Force(kN, mean±SD)			
Level	L1-L5	L1-L3	L4-L5
PS	1.399±0.28	1.206±0.19	1.641±0.19
Fuse	0.852±0.21	0.751±0.22	0.980±0.13
p Value	<0.001	0.005	0.002
Stiffness(kN/mm, mean±SD)			
Level	L1-L5	L1-L3	L4-L5
PS	1.275±0.16	1.151±0.1	1.429±0.08
Fuse	0.431±0.11	0.413±0.13	0.4549±0.08
p Value	<0.001	0.002	0.001

Table 6. Group 2 peak force and stiffness comparison between PS and Capstone cage with subgroup analysis for the upper lumbar spine(L1-L3) and lower lumbar spine (L4-L5).

Patient-Specific x Capstone Cage			
Peak Force(kN, mean±SD)			
Level	L1-L5	L1-L3	L4-L5
PS	1.381±0.50	1.315±0.54	1.465±0.45
Capstone	1.164±0.48	1.261±0.47	1.044±0.47
p Value	0.0865	0.75167	0.01433
Stiffness(kN/mm, mean±SD)			
Level	L1-L5	L1-L3	L4-L5
PS	1.382±0.47	1.263±0.4	1.530±0.5
Capstone	0.867±0.45	0.855±0.33	0.883±0.56
p Value	0.00885	0.063	0.107

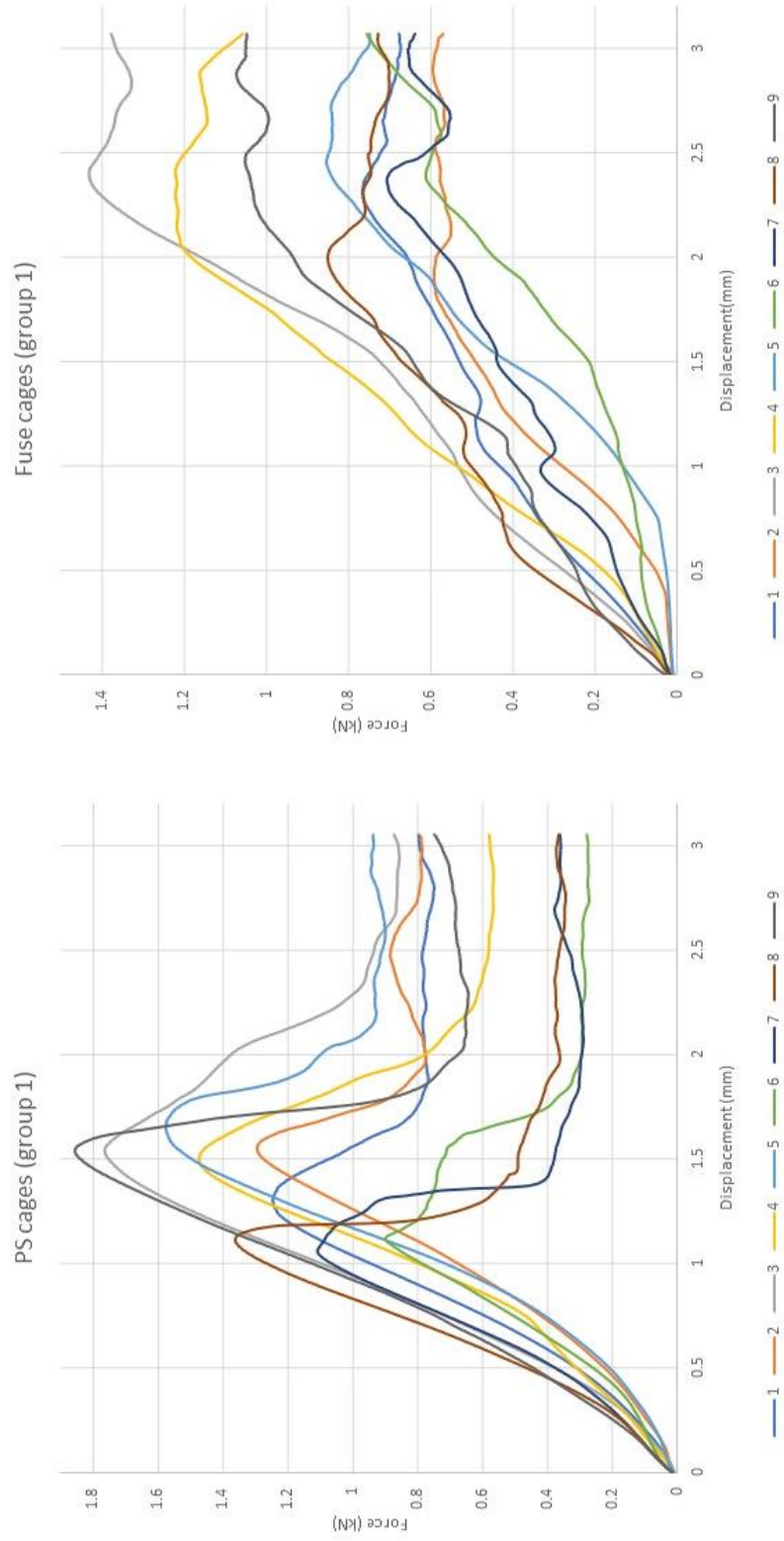


Figure 20. Force-displacement plots for PS and Fuse cage in group 1.

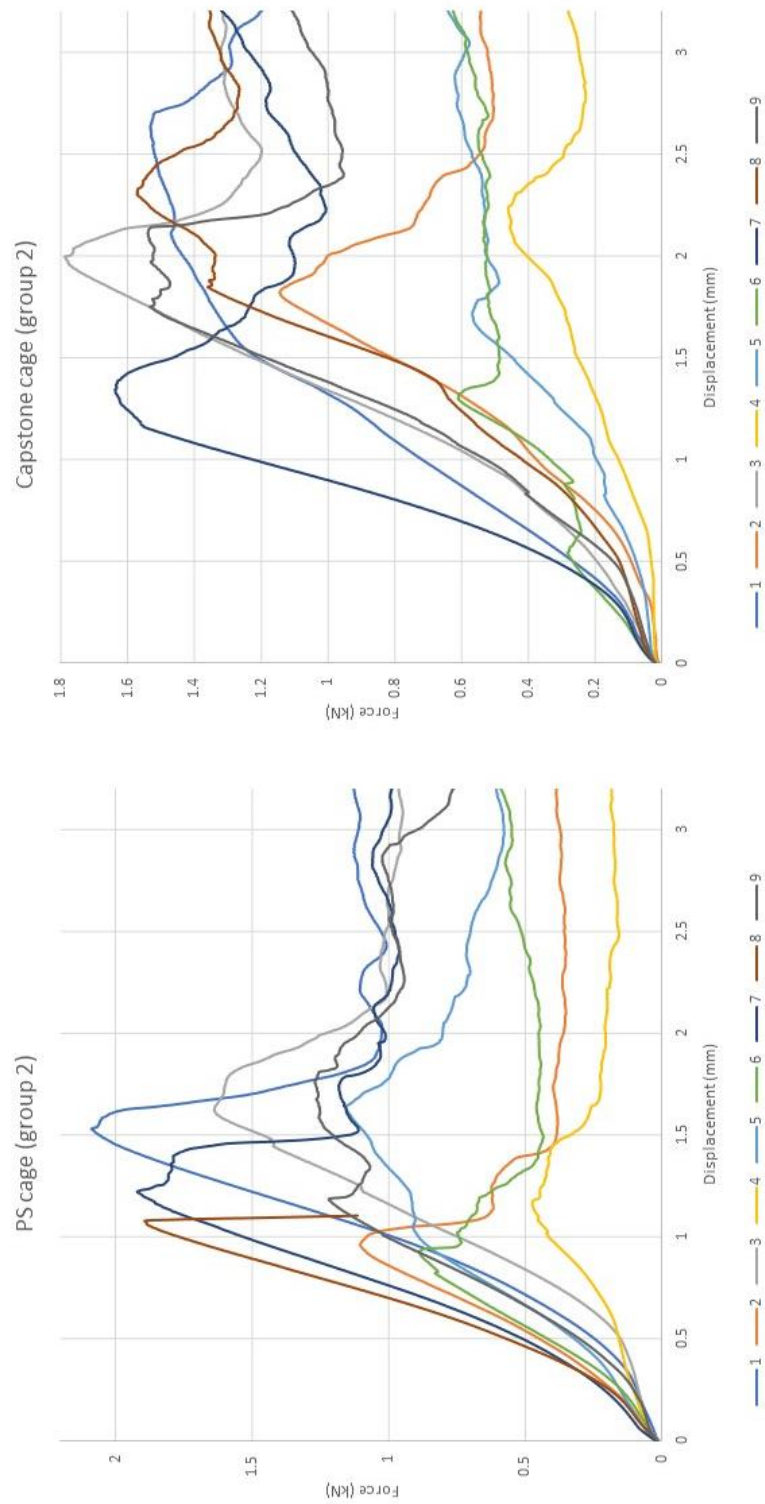


Figure 21. Force-displacement plots for PS and Capstone cage in group 2.

Discussion

This study's main findings showed that PLIF patient-specific cages could be up to 1.6 times stiffer than the commercially available cages used for this study, and they required up to 64% more force to subside. The study compared IFDs developed to match the endplate contour to two types of cages widely used for PLIF procedures and provides concrete biomechanical evidence of 3D printed devices' superiority.

Choi et al. described subsidence as being an incorporation process of the cages to the endplates that increases contact with the bone(18). However, it causes a reduction in the disc space and foraminal height. Therefore, better strategies to avoid subsidence and increase contact area are needed.

Yuan et al.(7) showed that larger LLIF cages could reduce subsidence risk compared to smaller PLIF cages due to the cages' increased surface area. However, larger cages cannot be inserted through the posterior approaches due to the limited dissection corridor used in such approaches (19). This corresponds to the vast majority of interbody fusion surgeries(20). As an alternative, using a device that matches the endplate surface shape can allow for an increased area of contact between the cage and the endplate, thereby reducing the risk of subsidence.

Previous studies using finite element analysis showed that patient-specific cages could reduce the stress distribution across the cage and endplate surface; therefore, they reduce subsidence risk(9-11). The main drawback of finite element analysis is that the models are expected to have a perfect match to the 3D endplate cross-section area. It has been shown that there are size and volume differences between the CT scan-based 3D-model and the human bone(13). The present study demonstrated that the biomechanical superiority is

maintained for the 3D printed models, even though a mismatch may remain between the cage surface area and the bone. Also, Wang et al.(21) showed that the cranial endplates were deeper at the lower lumbar spine levels (L4-L5) than the upper lumbar vertebrae (L1-L3). A subgroup analysis in our study showed that the patient-specific cages had a better performance in relation to the commercial cages when considering the lower levels of the lumbar spine in relation to the upper levels (Tables 1 and 2).

Also, subsidence risks increase due to the mismatch between the endplate elastic modulus and the cages' material elastic modulus (22). Titanium cages are more prone to subside than PEEK cages due to the higher elastic modulus(9). All the cages were printed in a resin with an elastic modulus similar to PEEK for this study. The material is resistant to deformation, allowing standardization of the material, and reducing costs and turnaround time.

Bone mineral density(BMD) can negatively affect endplate properties and increase subsidence risk (6). We did not have BMD data for the cadavers in this study, but the PS cages and commercial cages were paired so that they would serve as their own control to avoid bias due to BMD differences.

When comparing the force-displacement plots (Figures 8 and 9) for the PS cages and the commercial cages, the PS cages curves are smoother than the commercial cages curves. It shows a better accommodation of the PS cage over the endplate since the beginning of the test compared to the commercially available cages.

We need to recognize the limitations of the study. In the first place, this is a cadaveric study that brings limitations in the number of specimens available for testing. The number of samples used for testing in each group was more than the recommended for biomechanical testing(17). Also, as an in-vitro cadaveric study, the careful process

involved in cleaning the endplates may not be reproduced in-vivo and can create distortions in the endplate surface.

Moreover, the 3D printing process itself can add errors to the cage's final aspect since the mere change in the device orientation in the printing platform can cause distortions related to the resin curing process. Also, the 3D printer definition is a limitation to the cage's contact surface final definition, but the CT-scan definition constraints are the bottleneck of the process. Even with the possible errors added to the PS cages, they performed better than the commercial cages.

During the process, only one cage size was used for all the vertebrae. Therefore, for smaller vertebral bodies, the cage could load the endplate's periphery, increasing the amount of force required for failure(23).

Another limitation is the fact that to ensure that the PS cages were placed in the planned position, we printed endplate guides. It is not feasible from a clinical perspective; thus, intraoperative navigation strategies would be required(24).

As an in-vitro test, the testing used constant and progressive loads in one direction and did not consider the cyclic shear forces involved in the lumbar spine movement. Also, only one endplate was evaluated. In a clinical scenario, the cage would have to match the same disc space's superior and inferior endplate contour.

Despite the possible mismatch between the CT-scan-based 3D model used for the PS cages planning and the errors added to the 3DP process, PS cages had a better performance than the commercial cages.

Conclusion

Patient-specific cages created using additive manufacturing were capable of increasing the load-sharing across the endplate in relation to commercially available non-patient-specific cages. They required higher compression forces to produce failure and increased the cage-endplate construct's stiffness, decreasing subsidence risk.

References

1. Martin BI, Mirza SK, Spina N, Spiker WR, Lawrence B, Brodke DS. Trends in Lumbar Fusion Procedure Rates and Associated Hospital Costs for Degenerative Spinal Diseases in the United States, 2004 to 2015. *Spine (Phila Pa 1976)*. 2019;44(5):369-76.
2. Formica M, Vallerga D, Zanirato A, Cavagnaro L, Basso M, Divano S, et al. Fusion rate and influence of surgery-related factors in lumbar interbody arthrodesis for degenerative spine diseases: a meta-analysis and systematic review. *Musculoskelet Surg*. 2020;104(1):1-15.
3. Spiker WR, Goz V, Brodke DS. Lumbar Interbody Fusions for Degenerative Spondylolisthesis: Review of Techniques, Indications, and Outcomes. *Global Spine J*. 2019;9(1):77-84.
4. Patel DV, Yoo JS, Karmarkar SS, Lamoutte EH, Singh K. Interbody options in lumbar fusion. *J Spine Surg*. 2019;5(Suppl 1):S19-s24.
5. Lee N, Kim KN, Yi S, Ha Y, Shin DA, Yoon DH, et al. Comparison of Outcomes of Anterior, Posterior, and Transforaminal Lumbar Interbody Fusion Surgery at a Single Lumbar Level with Degenerative Spinal Disease. *World Neurosurg*. 2017;101:216-26.
6. Oh KW, Lee JH, Lee JH, Lee DY, Shim HJ. The Correlation Between Cage Subsidence, Bone Mineral Density, and Clinical Results in Posterior Lumbar Interbody Fusion. *Clin Spine Surg*. 2017;30(6):E683-e9.
7. Yuan W, Kaliya-Perumal AK, Chou SM, Oh JY. Does Lumbar Interbody Cage Size Influence Subsidence? A Biomechanical Study. *Spine (Phila Pa 1976)*. 2020;45(2):88-95.
8. Wallace N, Schaffer NE, Aleem IS, Patel R. 3D-printed Patient-specific Spine Implants: A Systematic Review. *Clin Spine Surg*. 2020;33(10):400-7.
9. Chatham LS, Patel VV, Yakacki CM, Dana Carpenter R. Interbody Spacer Material Properties and Design Conformity for Reducing Subsidence During Lumbar Interbody Fusion. *J Biomech Eng*. 2017;139(5):0510051-8.
10. Patel RR. Does patient-specific implant design reduce subsidence risk in lumbar interbody fusion? A bottom up analysis of methods to reduce vertebral endplate stress. Denver, CO: University of Colorado Denver; 2018.
11. Zhang M, Pu F, Xu L, Zhang L, Liang H, Li D, et al. Development of an integrated CAD-FEA system for patient-specific design of spinal cages. *Comput Methods Biomech Biomed Engin*. 2017;20(4):355-64.
12. Kanawati A, Rodrigues Fernandes RJ, Gee A, Urquhart J, Siddiqi F, Gurr K, et al. The Development of novel 2-in-1 patient specific, 3D-printed laminectomy guides with integrated pedicle screw drill guides. *World Neurosurgery*. 2021.
13. Kanawati A, Fernandes RJ, Gee A, Urquhart J, Siddiqi F, Gurr K, et al. Geometric and Volumetric Relationship Between Human Lumbar Vertebra and CT-based Models. *Acad Radiol*. 2020.
14. Calignano F, Galati M, Iuliano L, Minetola P. Design of Additively Manufactured Structures for Biomedical Applications: A Review of the Additive Manufacturing Processes Applied to the Biomedical Sector. *J Healthc Eng*. 2019;2019:9748212.
15. Galvez M, Montoya CE, Fuentes J, Rojas GM, Asahi T, Currie W, et al. Error Measurement Between Anatomical Porcine Spine, CT Images, and 3D Printing. *Acad Radiol*. 2020;27(5):651-60.
16. Goh JC, Wong HK, Thambyah A, Yu CS. Influence of PLIF cage size on lumbar spine stability. *Spine (Phila Pa 1976)*. 2000;25(1):35-9; discussion 40.

17. ASTM F2267-04(2018), Standard Test Method for Measuring Load Induced Subsidence of Intervertebral Body Fusion Device Under Static Axial Compression, ASTM International, West Conshohocken, PA, 2018, www.astm.org.
18. Choi JY, Sung KH. Subsidence after anterior lumbar interbody fusion using paired stand-alone rectangular cages. *Eur Spine J.* 2006;15(1):16-22.
19. Mobbs RJ, Phan K, Malham G, Seex K, Rao PJ. Lumbar interbody fusion: techniques, indications and comparison of interbody fusion options including PLIF, TLIF, MI-TLIF, OLIF/ATP, LLIF and ALIF. *J Spine Surg.* 2015;1(1):2-18.
20. Goz V, Weinreb JH, Schwab F, Lafage V, Errico TJ. Comparison of complications, costs, and length of stay of three different lumbar interbody fusion techniques: an analysis of the Nationwide Inpatient Sample database. *Spine J.* 2014;14(9):2019-27.
21. Wang Y, Battié MC, Videman T. A morphological study of lumbar vertebral endplates: radiographic, visual and digital measurements. *Eur Spine J.* 2012;21(11):2316-23.
22. Tan JS, Bailey CS, Dvorak MF, Fisher CG, Oxland TR. Interbody device shape and size are important to strengthen the vertebra-implant interface. *Spine (Phila Pa 1976).* 2005;30(6):638-44.
23. Cadman J, Sutterlin C, 3rd, Dabirrahmani D, Appleyard R. The importance of loading the periphery of the vertebral endplate. *J Spine Surg.* 2016;2(3):178-84.
24. Joseph JR, Smith BW, Patel RD, Park P. Use of 3D CT-based navigation in minimally invasive lateral lumbar interbody fusion. *J Neurosurg Spine.* 2016;25(3):339-44.

Chapter 5 – Conclusion and future directions

This research aimed to investigate biomechanical strategies that aid in reducing subsidence in posterior lumbar interbody fusion surgery. Although different techniques are available for the insertion of cages into the disc space, this research's emphasis was PLIF surgery since it is the most commonly used technique among spine surgeons.

The first chapter highlighted that, although the PLIF technique was described approximately 60 years ago, the use of interbody cages to enhance bone fusion, correct spine malalignment and help in the decompression of neural elements is relatively new. Also, the introduction chapter intended to promote an overview of the main complication after interbody fusion surgery and the work done so far to try to reduce its occurrence.

Chapter 2 investigated the role of morselized bone graft packed within the cage to prevent subsidence and determine if the compression force used to load the morselized bone graft influences mechanical support to minimize cage subsidence. A titanium mesh cage with thin walls was used to reduce the cage's influence on the overall construct so that a more accurate evaluation of the bone graft behaviour could be performed. The results showed that the bone graft could be used as a structural component to increase the load sharing between the cage and the graft and reduce the construct's contact stress, thereby reducing the risk of subsidence. According to Wolff's law, higher compression of the bone graft should promote a better environment for bone fusion to occur, but further studies are necessary to validate this hypothesis. Although a titanium mesh cage was used in this study, the results can be applied to every cage having a space for the bone graft since the graft area typically accounts for a fair amount of the cage's total area.

In chapter 3, the mismatch between the 3D cage model obtained from the CT-scan 3D volumetric reconstruction of the vertebral body and the cadaveric bone was explored. The study showed that patient-specific cages did not reach 100% contact and therefore provides evidence that a mismatch between the CT-image endplate and the bone endplate contour exists. This mismatch occurs due to limitations in CT-scan image resolution used for clinical image acquisition and 3D printer resolution. Nonetheless, the patient-specific cages succeeded in achieving more contact between the cage and the endplate when compared to the commercial cages tested in this study. There is a lack of studies investigating the differences between the human bone endplate and the image obtained using CT-scan or magnetic resonance imaging(MRI). Further studies using spatial analysis would be necessary to describe the endplate morphology in better detail.

Chapter 4 is the first study to compare the in-vitro biomechanical behaviour of 3D printed patient-specific cages matching the endplate surface compared to previous studies that only used finite element models. It consisted of a biomechanical load test to endplate failure using patient-specific cages and commercial cages. In line with the previous chapter, the increase in the patient-specific cage's contact area resulted in a stiffer construct that required a higher amount of force for subsidence to occur. The study provides valuable information about the biomechanical superiority of devices matching the patient's endplate anatomy and can be used to drive further studies about optimal implant design.

Appendix A

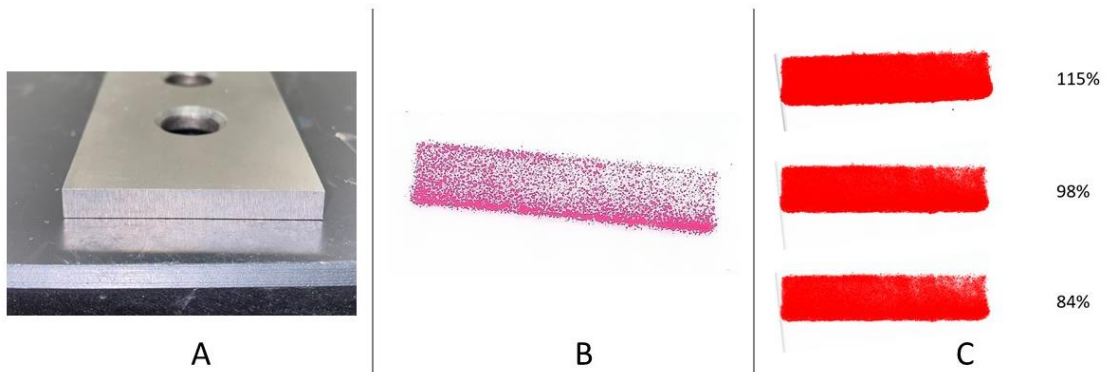
Pressure-sensitive film calibration

During pressure-sensitive film analysis, the total contact area measured is based on the stain produced after the compression testing and the stain's pressure is measured based on the colour intensity. Using the software ImageJ, the number of stained pixels can be counted and transformed in the total area of contact corresponding to the pixels' number. In order to make this possible, a flat object (Figure 1A) with a known area was compressed over the film to reproduce its image.

The film in which the stain was registered was scanned in jpeg format (Figure 1B) at 1200 dpi (dots per inch) using a desktop scanner (Hewlett-Packard, HP ENVY 4520).

To obtain the total area of the object, the thresholding tool in ImageJ was used. It is adjusted by choosing a value cutoff, such that every pixel less than a specific value is excluded, while every pixel greater than that value is considered for the analysis.

The value cutoff was chosen based on the pixel count when at least 95%, but less than 100% of the known area was obtained. This methodology avoids false-positive values in the total area being measured by not considering lightly touched areas (Figure 1C).



Curriculum Vitae

Renan Jose Rodrigues Fernandes

Orthopedic Surgeon

2021

Degrees

2014/3 - 2017/2 Bachelor's, Orthopaedic Surgeon, Universidade de Sao Paulo

2008/2 - 2013/11 Bachelor's, Doctor of Medicine, Universidade de Sao Paulo

Credentials

2019/3 Spine Surgeon, Universidade de Sao Paulo

2017/3 Orthopaedic and Traumatology Board Certification, Brazilian Society of Orthopaedics and Traumatology

Employment

2017/3 - 2019/6 Orthopaedic and Trauma surgeon - Hospital Estadual de Sapopemba

2018/6 - 2019/5 Spine Surgeon - Clinica Ortopedica OrtoCity

Affiliations

2020/7 - 2022/6 Spine Surgery Clinical Fellow, University of Western Ontario

2019/7 - 2020/6 Research fellow, University of Western Ontario

Other Memberships

2017/3 Member, Brazilian Society of Orthopedics and Traumatology

Publications

Journal Articles

1. (2021). Geometric and volumetric relationship between human lumbar vertebrae and 'Black-bone' MRI-based models. *The international journal of Medical Robotics and Computer-Assisted Surgery*. <https://doi.org/10.1002/rcs.2220>
2. Patel M, Martin J, Campbell D, Fernandes R, Amini M. (2020). Inferior Tilt of the Glenoid Increases Impingement in Reverse Shoulder Arthroplasty. *Journal of Shoulder and Elbow Surgery*. <https://doi.org/10.1016/j.jse.2020.09.023>
3. Tavares Junior M, Sanchez F, Iturralde D, Fernandes R, Marcon R, Cristante A, Barros Filho T, Letaif O. (2020). Comparative tomographic study of the iliac screw and the S2-alar-iliac screw in children. *Clinics*. 75(1824) <http://dx.doi.org/10.6061/clinics/2020/e1824>
4. Saruhashi M, Videira L, Santos A, Lucarini B, Fernandes R, Giglio P, Pecora J, Camanho G, Hinckel B, Gobbi R. (2020). Anatomical risk factors for anterior cruciate ligament injury are not important as patellar instability risk factors in patients with acute knee injury. *The Journal of Knee Surgery*. <https://doi.org/10.1055/s-0040-1716504>
5. Kanawati A, Fernandes R, Gee A, Urquhart J, Siddiqi F, Gurr K, Bailey C, Rasoulinejad P. (2020). Geometric and volumetric relationship between human lumbar vertebra and CT based models. *Academic Radiology*. <https://doi.org/10.1016/j.acra.2020.05.027>
6. Kanawati A, Fernandes R, Gee A, Urquhart J, Rasoulinejad P, Bailey C. (2020). Anatomical relationship between the accessory process of the lumbar spine and the pedicle screw entry point. *Clinical Anatomy*. <http://dx.doi.org/10.1002/ca.23658>
7. Silva R, Fernandes R, Ono A, Marcon R, Cristante A, Barros Filho T. (2017). Role of different hormones in the pathogenesis and severity of adolescent idiopathic scoliosis. *Acta Ortopedica Brasileira*. 25(1): 15-17.